SIAM J. APPL. MATH.
Vol. 52, No. 6, pp. 1533–1562, December 1992

003



# NUMERICAL SIMULATION OF THE MOTION OF RIGID SPHERES IN POTENTIAL FLOW*

HYUN S. KIM†‡ AND ANDREA PROSPERETTI†

**Abstract.** A numerical method for the simulation of the motion of a number of rigid spheres in a potential flow is described. The equations derived are applicable to the case of spheres in an unbounded fluid or in a circular tube of variable cross section. The method itself is, however, more general and can be applied to a variety of situations. The maximum number of spheres is only limited by the available computational resources. Some numerical examples are described both as a test of the method and for their intrinsic interest. The ultimate aim of the study is to develop a tool capable of shedding light on the nature of the inertial coupling in two-phase disperse flows.

**Key words.** multiparticle simulation, potential flow, two-phase flows

**AMS(MOS) subject classifications.** 76B99, 76T05, 65C20

## 1. Introduction.

Except in the simplest cases, the study of flows involving more than one phase must be based on averaged equations (see, e.g., Drew [13], Drew and Wood [14], Hinch [17], Ishii [20], Nigmatulin [26]). As in the case of turbulence, this approach leads to a closure problem in the sense that, as a consequence of averaging, quantities are introduced that are not exactly expressible in terms of the primary averaged variables (see, e.g., Bouré [8]). It is therefore necessary to introduce further equations to balance the number of unknowns. While this objective can be achieved exactly in particular cases (for small volume fractions of the dispersed phase, see Batchelor and Green [4], Biesheuvel and van Wijngaarden [7], Caflisch et al. [10], Hinch [17], Rubinstein [28]; for small-amplitude surface deformation of stratified flows, see Banerjee [2]; for small disturbances, see Caflisch et al. [10], Sangani [29]; and others), typically the domain of validity of these exact results is quite limited and falls far short of many, if not most, situations of practical interest.

Aside from concerns of physical realism, the closure issue is critical also for another reason, namely, the fact that most of the averaged equations exhibit a tendency toward instability, which renders their numerical solution problematic (see, e.g., Jones and Prosperetti [21], Prosperetti and Jones [27]).

It is against this backdrop that the current efforts at the direct numerical simulation of two-phase flows can be properly appreciated. Here particle motions are tracked individually by computer to generate a large body of data from which, it is hoped, information useful for the closure problem can be extracted. This approach is similar in its philosophy to physical experimentation, but, for certain purposes, it enjoys several advantages over the latter. Indeed, the amount of data generated numerically is orders of magnitude greater than what would be possible in the laboratory, a very detailed control of the "experiment" is possible, and the physical effects that operate concurrently in nature can be separated to ascertain their importance and facilitate their modelling.

* Received by the editors June 10, 1991; accepted for publication (in revised form) February 4, 1992. This study was supported in part by Department of Energy, Office of Basic Energy Sciences grant DE-FG02-89ER14043 and by National Science Foundation grant CBT-8918144.

† Department of Mechanical Engineering, The Johns Hopkins University, Baltimore, Maryland 21218.

‡ Present address, Acoustics Laboratory, Korea Research Institute of Ships and Ocean Engineering, Daeduk Science Town, P.O. Box 1, Daejeon, 305-606, Korea.

The approach originated in plasma physics in the late 1960s (Hockney and Eastwood [18]) and has recently become quite widespread in the theory of liquids (Abraham [1], Hoover [19]), in the theory of granular flows (Campbell [12], Walton and Braun [35]), in low-Reynolds number (Brady and Bossis [9], Durlofsky, Brady, and Bossis [15], Sangani and Acrivos [31], Sangani and Didwania [32]), and in high-Reynolds number disperse two-phase flow (Sangani, Zhang, and Prosperetti [34]). In this paper, it is applied to the *inertial coupling* of particles dispersed in inviscid, incompressible flow. It is not our purpose here to suggest closure relations of the averaged equations applicable to large Reynolds number flows. This remains a long-term objective, which, it should be clearly stated, is the *main* justification of the present work. Rather, we present some analytical and numerical methods suitable for the simulation of the motion of rigid spheres in potential flow. Cases of unbounded fluids as well as of flow in the presence of boundaries, such as through a nozzle, are considered. The results of the systematic applications of these techniques will be reported in future studies. Here we only give some illustrative examples.

The motion of noninteracting spheres in potential flow is, of course, one of the early applications of fluid mechanics. The motion of pairs of spheres sufficiently far apart to interact only weakly also received attention over a century ago (Bassett [3], Milne-Thomson [25]). The study of strongly interacting sphere pairs is, however, a relatively recent development (van Wijngaarden [36], Biesheuvel and van Wijngaarden [6], Kok [24]) undertaken with the purpose of obtaining a closure of the averaged equations of disperse two-phase flows valid to second order in the spheres' volume fraction $\beta$. van Wijngaarden [36] derived an order-$\beta$ correction to the single-sphere added mass coefficient, which was more recently reconsidered and refined (Biesheuvel and Spoelstra [5] and Kok [24]). Biesheuvel and van Wijngaarden [7] used this approach to obtain an order-$\beta^2$ expression for the averaged convective flux of momentum.

Extension of these results to larger volume fractions cannot be accomplished by the techniques used by these authors. A numerical approach is necessary. Sangani and Yao [33] have developed a method based on a multipole expansion of the potential and have applied it to the problem of heat conduction in a composite. That study has led to work on small-amplitude oscillatory flows described by Sangani [30] and Sangani, Zhang, and Prosperetti [34]. The approach developed here is somewhat different, as it deals with the values of the potential on the different surfaces bounding the flow. A complete elucidation of the advantages and disadvantages of the two approaches cannot be obtained on the basis of the presently available limited experience and must await further research.

Another important point that is left open here is the development of efficient numerical techniques, exact or approximate. For example, Durlofsky, Brady, and Bossis [15] have proposed an approach that effectively combines long-range approximations (incorporating multiple-body interactions) with exact pairwise interactions at small separations. Karrila and Kim [23] have developed methods designed to exploit most efficiently the available massively parallel computers, and Greengard and Rokhlin [16] have formulated efficient techniques for the calculation of potential fields. Before similar developments are attempted on the present approach, we feel that it is important to possess a simple, reliable, and robust numerical technique that can be used as a benchmark against which to compare them. It is such a technique that is outlined in the present paper.

To illustrate the method, we consider several examples of massless spheres ("bubbles") carried by a flow through a converging-diverging nozzle in a pipe, and of spheres moving under the action of buoyancy.

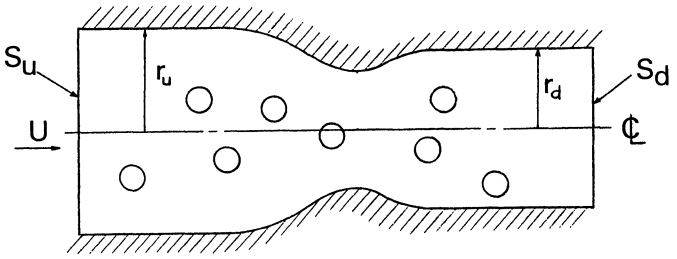


FIG. 1. *The potential flow of rigid spheres in a tube considered in this paper.*

**2. Mathematical formulation.** The situation we model is that of a pipe of uniform cross section upstream $S_u$ and downstream $S_d$ of a nozzle or other constriction (Fig. 1). For simplicity, we take the pipe's cross section to be circular, although the method can be extended to more general situations. The mixture flowing in the pipe consists of spheres suspended in an inviscid incompressible fluid. Since our emphasis here is on the study of the inertial coupling between the disperse and continuous phases, we take the fluid flow to be potential and the spheres to be rigid, massless, and with the same radius $a$. The number of spheres the center $\mathbf{x}^\alpha$ of which is contained in the region between $x_u$ and $x_d$ is denoted by $N_S$, which may depend on time. Greek indices ranging between 1 and $N_S$ are used to label the spheres.

Let $S_u U$ be the (possibly time-dependent) volumetric flow rate of the liquid-spheres mixture in the upstream section of the tube. Then we begin by writing the total liquid velocity potential $\phi_T$ as

$$\phi_T(\mathbf{x}) = U\,x + \phi(\mathbf{x}), \tag{1}$$

where $x$ is a coordinate measured along the axis of the tube and $\phi(\mathbf{x})$ represents the potential of the disturbance due to the relative motion of the particles with respect to the liquid and the variations of the tube's cross section. The time dependence enters parametrically in the problem for the velocity potential and is understood for simplicity of writing. We assume that the particles move with the fluid upstream of the constriction, and therefore $\phi \to 0$ at upstream infinity, $x \to -\infty$.

Downstream of the flow constriction, $x \to \infty$, we impose

$$\phi \sim C + \Delta U\,x, \tag{2}$$

with $C$ a constant to be determined and $\Delta U$ given from the condition of conservation of the total volumetric flow rate through the tube,

$$\Delta U = \left(\frac{S_u}{S_d} - 1\right) U. \tag{3}$$

If the downstream cross section is equal to the upstream one, then both liquid and spheres must move at the same velocity $U$ downstream, and condition (2) is exact. If, however, $S_u \neq S_d$, (2) is only correct until the first sphere arrives in the neighborhood of the point where it is imposed.

Consider now a section of the tube delimited by two cross sections (again denoted by $S_u$ and $S_d$) orthogonal to its axis, respectively, upstream and downstream of the flow constriction, and write Green's identity for $\phi(\mathbf{x})$

$$2\pi\gamma\phi(\mathbf{x}) = \int_S \left[-\phi(\mathbf{x}')\frac{\partial}{\partial n'}\frac{1}{|\mathbf{x}-\mathbf{x}'|} + \frac{\partial\phi(\mathbf{x}')}{\partial n'}\frac{1}{|\mathbf{x}-\mathbf{x}'|}\right] dS(\mathbf{x}'). \tag{4}$$

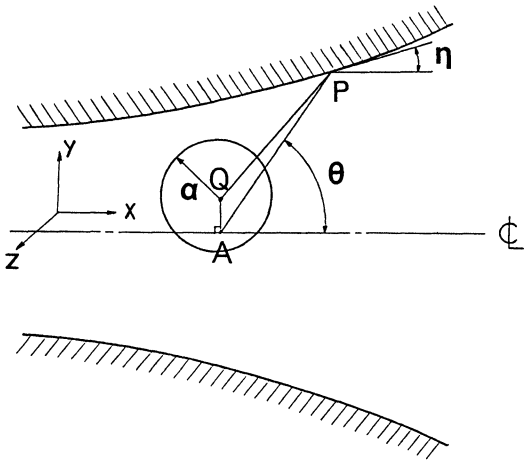


FIG. 2. *Definition of the angle $\eta$ first appearing in* (6) *and of the geometry used in* §3.1.

Here $S$ denotes the boundary of the domain occupied by the fluid and consists of the upstream and downstream cross sections $S_u$ and $S_d$, the tube's wall $S_W$, and the surfaces of the spheres $S^\alpha$, $\alpha = 1, 2, \cdots, N_S$, so that

$$\int_S = \int_{S_W} + \int_{S_u} + \int_{S_d} + \sum_{\alpha=1}^{N_S} \int_{S^\alpha}. \tag{5}$$

In (4) the parameter $\gamma$ is defined in such a way that $2\pi\gamma$ represents the solid angle under which the domain occupied by the fluid is seen from the field point $\mathbf{x}$. Hence, $\gamma = 2$ if $\mathbf{x}$ is a point interior to the fluid domain, $\gamma = \frac{1}{2}$ if $\mathbf{x}$ belongs to the circles where $S_u$ or $S_d$ intersect $S_W$, and, provided that the pipe cross section varies smoothly, $\gamma = 1$ for $\mathbf{x}$ any other point of $S$. Our approach is to regard (4) as an integral equation for the disturbance potential. When this quantity has been determined, as is shown in §4, it is possible to calculate the motion of the spheres.

We now write (4) in a more explicit form. On the surface $S_W$ of the pipe, the normal component of the fluid velocity vanishes, which leads to

$$\frac{\partial \phi}{\partial n} = -U \frac{\partial x}{\partial n} = U \sin \eta, \tag{6}$$

where $\eta$ denotes the angle that the tangent to the pipe's trace with a meridian plane through the axis makes with the axis (Fig. 2). On the surface of the sphere $\alpha$,

$$\frac{\partial \phi}{\partial n} = \mathbf{V}^\alpha \cdot \mathbf{n} - U \frac{\partial x}{\partial n}, \tag{7}$$

where $\mathbf{V}^\alpha$ is the translational velocity of the sphere $\alpha$.

It proves convenient for the following developments to use several different coordinate systems. The first one is Cartesian, with the $x$-axis in the direction of the flow along the pipe's axis, the $y$-axis in the meridian plane (the plane of Fig. 2), and the $z$-axis orthogonal to the meridian plane. Second, we use a cylindrical coordinate system $(r, x, \psi)$ centered on the $x$-axis with the angular coordinate measured from the $(x, y)$ meridian plane. Third, we use spherical coordinate systems $(r^\alpha, \theta^\alpha, \psi^\alpha)$

centered at the center $\mathbf{x}^\alpha$ of each sphere with the polar axis parallel to the $x$-axis and $\psi^\alpha$ measured from the plane containing the polar and the pipe's axes. In terms of these "local" polar coordinates, the previous kinematic boundary condition on the surface of the sphere $\alpha$, (7), becomes

$$\frac{\partial \phi}{\partial n} = (U - V_x^\alpha)\cos\theta^\alpha - V_y^\alpha \sin\theta^\alpha \cos\psi^\alpha - V_z^\alpha \sin\theta^\alpha \sin\psi^\alpha, \tag{8}$$

where $V_x^\alpha$, $V_y^\alpha$, and $V_z^\alpha$ are the components of $\mathbf{V}^\alpha$ in the Cartesian coordinate system.

Finally, we take the surface $S_u$ far enough upstream of the flow constriction that we can take $\phi = 0, \partial\phi/\partial n = 0$ there. Similarly, on $S_d$, we assume that $\phi = C + \Delta U x_d$ and (the average value of) $\partial\phi/\partial n = \Delta U$, where $x_d$ is the abscissa of $S_d$. Although, strictly speaking, these are over-specifications for the elliptic problem at hand, the procedure is legitimate provided that $S_u$ and $S_d$ are taken sufficiently far away from the region of the constriction.

With the previous assumptions and specifications, (4) then becomes

$$\begin{aligned} 2\pi\gamma\phi(\mathbf{x}) = &- \int_{S_W+S_d} \phi(\mathbf{x}')\frac{\partial}{\partial n'}\frac{1}{|\mathbf{x}-\mathbf{x}'|}dS(\mathbf{x}') \\ &+ U\int_{S_W}\frac{\sin\eta}{|\mathbf{x}-\mathbf{x}'|}dS(\mathbf{x}') \\ &+ \Delta U\int_{S_d}\frac{1}{|\mathbf{x}-\mathbf{x}'|}dS(\mathbf{x}') \\ &+ \sum_{\alpha=1}^{N_S}\int_{S^\alpha}\left[\frac{\mathbf{V}'^\alpha\cdot\mathbf{n}'}{|\mathbf{x}-\mathbf{x}'|} - \phi(\mathbf{x}')\frac{\partial}{\partial n'}\frac{1}{|\mathbf{x}-\mathbf{x}'|}\right]dS(\mathbf{x}'), \end{aligned} \tag{9}$$

in which $\mathbf{V}'^\alpha$ denotes $(V_x^\alpha - U, V_y^\alpha, V_z^\alpha)$.

**3. Solution procedure.** Equation (9) can be recast in a form more suitable for an efficient numerical solution as follows. First, we expand the value $\phi^\alpha$ of the disturbance potential on the surface of the sphere $\alpha$ in a series of spherical harmonics,

$$\phi^\alpha = \sum_{n=1}^{\infty}\sum_{m=0}^{n}[B_{nm}^\alpha(t)Y_n^m(\theta^\alpha,\psi^\alpha) + \tilde{B}_{nm}^\alpha(t)\tilde{Y}_n^m(\theta^\alpha,\psi^\alpha)], \tag{10}$$

where

$$\begin{aligned} Y_n^m(\theta^\alpha,\psi^\alpha) &= \frac{(n-m)!}{(n+m)!}P_n^m(\cos\theta^\alpha)\cos m\psi^\alpha, \\ \tilde{Y}_n^m(\theta^\alpha,\psi^\alpha) &= \frac{(n-m)!}{(n+m)!}P_n^m(\cos\theta^\alpha)\sin m\psi^\alpha, \end{aligned} \tag{11}$$

and the $P_n^m$'s are associated Legendre functions.

Similarly, on the surface of the pipe, we assume that $\phi$ can be expanded in Fourier series,

$$\phi(\mathbf{x},t) = \Phi_0(x,t) + \sum_{n=1}^{\infty}\left[\Phi_n(x,t)\cos n\psi + \tilde{\Phi}_n(x,t)\sin n\psi\right]. \tag{12}$$

By taking suitable scalar products of (9), we now obtain a system of equations for the coefficients $B_{nm}^\alpha, \tilde{B}_{nm}^\alpha, \Phi_n, \tilde{\Phi}_n$ of the above expansions.

**3.1. Field point on the pipe's wall.** When the field point $\mathbf{x}$ in (9) is taken on the pipe's wall, we multiply this equation by $\cos l\psi$ or $\sin l\psi$ and integrate over $\psi$ from 0 to $2\pi$ to find, respectively, that

$$
\begin{aligned}
2\pi^2\epsilon_l\gamma\Phi_l = &-\int_{x_u}^{x_d}\Psi_l(x,x',t)\frac{r'\,dx'}{\cos\eta}-\int_0^{r_d}\Psi_l(x,x',t)r'\,dr'\\
&+4\pi U\epsilon_l\delta_{l,0}\int_{x_u}^{x_d}\tan\eta\frac{K(m)}{A^{1/2}}r'\,dx'\\
&+4\pi\Delta U\epsilon_l\delta_{l,0}\int_0^{r_d}\frac{K(m)}{A^{1/2}}r'\,dr'\\
&-v\sum_{\alpha=1}^{N_S}\left\{\left[(V_x^\alpha-U)F_{C10}^{\alpha l}-2V_y^\alpha F_{C11}^{\alpha l}-2V_z^\alpha\tilde F_{C11}^{\alpha l}\right]\right\}\\
&+\sum_{\alpha=1}^{N_S}\sum_{n=1}^{\infty}\frac{4n\pi}{2n+1}a^{n+1}\sum_{k=0}^{n}\left(B_{nk}^\alpha F_{Cnk}^{\alpha l}+\tilde B_{nk}^\alpha\tilde F_{Cnk}^{\alpha l}\right)
\end{aligned}
\tag{13}
$$

and

$$
\begin{aligned}
2\pi^2\gamma\tilde\Phi_l = &-\int_{x_u}^{x_d}\tilde\Psi_l(x,x',t)\frac{r'\,dx'}{\cos\eta}-\int_0^{r_d}\tilde\Psi_l(x,x',t)r'\,dr'\\
&-v\sum_{\alpha=1}^{N_S}\left\{\left[(V_x^\alpha-U)F_{S10}^{\alpha l}-2V_y^\alpha F_{S11}^{\alpha l}-2V_z^\alpha\tilde F_{S11}^{\alpha l}\right]\right\}\\
&+\sum_{\alpha=1}^{N_S}\sum_{n=1}^{\infty}\frac{4n\pi}{2n+1}a^{n+1}\sum_{k=0}^{n}\left(B_{nk}^\alpha F_{Snk}^{\alpha l}+\tilde B_{nk}^\alpha\tilde F_{Snk}^{\alpha l}\right).
\end{aligned}
\tag{14}
$$

In these equations, $r'$ and $x'$ are the cylindrical coordinates of the source point $\mathbf{x}'$, $a$ is the radius of the spheres, $v$ is their volume, and

$$
\epsilon_0 = 2, \qquad \epsilon_l = 1 \ \text{ for } \ l \neq 0. \tag{15}
$$

The complete elliptic integral of the first kind is denoted by $K(m)$ with $m$ and $A$ defined by

$$
m = \frac{4r'r}{A}, \qquad A = (x-x')^2+(r+r')^2. \tag{16}
$$

The other quantities appearing in (13) and (14) are as follows. The functions $\Psi_l$ and $\tilde\Psi_l$ are defined by

$$
\Psi_l = \int_0^{2\pi}\int_0^{2\pi}\sum_{n=0}^{\infty}\left(\Phi_n\cos n\psi'+\tilde\Phi_n\sin n\psi'\right)\left(\frac{\partial}{\partial n'}\frac{1}{|\mathbf{x}-\mathbf{x}'|}\right)\cos l\psi\,d\psi\,d\psi', \tag{17}
$$

$$
\tilde\Psi_l = \int_0^{2\pi}\int_0^{2\pi}\sum_{n=0}^{\infty}\left(\Phi_n\cos n\psi'+\tilde\Phi_n\sin n\psi'\right)\left(\frac{\partial}{\partial n'}\frac{1}{|\mathbf{x}-\mathbf{x}'|}\right)\sin l\psi\,d\psi\,d\psi'. \tag{18}
$$

The integrations appearing here can be carried out in closed form and the results expressed in terms of complete elliptic integrals as shown in the Appendix. The

functions $F^{\alpha l}_{Cnk}$, $F^{\alpha l}_{Snk}$ are defined by

$$F^{\alpha l}_{Cnk} = \int_0^{2\pi} \frac{Y^k_n(\theta^\alpha, \psi^\alpha)}{|\mathbf{x} - \mathbf{x}^\alpha|^{n+1}} \cos l\psi \, d\psi,$$
$$F^{\alpha l}_{Snk} = \int_0^{2\pi} \frac{Y^k_n(\theta^\alpha, \psi^\alpha)}{|\mathbf{x} - \mathbf{x}^\alpha|^{n+1}} \sin l\psi \, d\psi, \tag{19}$$

and similarly for $\tilde{F}^{\alpha l}_{Cnk}$, $\tilde{F}^{\alpha l}_{Snk}$ with the $Y$'s replaced by $\tilde{Y}$'s. Although these integrals could be calculated numerically, this procedure would be quite inefficient particularly for large values of $l$ and $k$. The difficulty in their analytical evaluation lies in the fact that, as mentioned before, the angle $\psi$ is measured from the meridian plane through the pipe's axis, while the angles $\psi^\alpha$ are the polar angles in the polar coordinate system of sphere $\alpha$. By using (A.24) of the Appendix, we can express the spherical harmonics $Y^k_n(\theta^\alpha, \psi^\alpha)/|\mathbf{x} - \mathbf{x}^\alpha|^{n+1}$ in terms of the angle $\psi$, after which the integrations indicated in these equations can be performed. The result is

$$F^{\alpha l}_{Cnk} = \epsilon_l \pi \sum_{n'=0}^{\infty} a^{n'}_{nk} \left[ \Gamma^0_A + \sum_{k'=1}^{n'} (\Gamma^{k'}_A + \Gamma^{k'}_B) \cos k'\xi \right],$$
$$\tilde{F}^{\alpha l}_{Cnk} = \epsilon_l \pi \sum_{n'=0}^{\infty} a^{n'}_{nk} \sum_{k'=1}^{n'} (\Gamma^{k'}_B - \Gamma^{k'}_A) \sin k'\xi,$$
$$F^{\alpha l}_{Snk} = \pi \sum_{n'=0}^{\infty} a^{n'}_{nk} \sum_{k'=1}^{n'} (\Gamma^{k'}_A + \Gamma^{k'}_B) \sin k'\xi, \tag{20}$$
$$\tilde{F}^{\alpha l}_{Snk} = \pi \sum_{n'=0}^{\infty} a^{n'}_{nk} \left[ \Gamma^0_A + \sum_{k'=1}^{n'} (\Gamma^{k'}_A - \Gamma^{k'}_B) \cos k'\xi \right],$$

where $\epsilon_l$ is as defined above in (15) and

$$a^{n'}_{nk} = \frac{(n-k)!}{(n+k)!} \frac{d^{n'}}{b^{n+n'+1}}, \tag{21}$$

$$\Gamma^{k'}_A = A^{nk}_{n'k'} P^{k'}_{n'}(0) P^{k+k'}_{n+n'}(\cos\theta) \delta_{k+k',l}, \tag{22}$$

$$\Gamma^{k'}_B = B^{nk}_{n'k'} P^{k'}_{n'}(0) P^{|k-k'|}_{n+n'}(\cos\theta) \delta_{|k-k'|,l}, \tag{23}$$

in which $A^{nk}_{n'k'}$ and $B^{nk}_{n'k'}$ are defined in the Appendix. In writing these expressions, we have used the polar coordinates of the points $P$ and $A$ in the spherical coordinate system centered at the point $Q$, the center of the sphere $\alpha$ (Fig. 2). The definitions are $Q - A = (d, \pi/2, \xi)$ and $P - Q = (R, \theta^\alpha, \psi^\alpha)$. In addition, we have set $P - A = (b, \theta, \psi)$. The point $A$ is chosen such that $Q - A$ is perpendicular to the symmetry axis of the pipe, which ensures that $d/b < 1$. For brevity, we have not appended all the indices appearing in the right-hand sides of their definitions to $\Gamma_A$ and $\Gamma_B$. This abbreviated notation is occasionally adopted in the following as well. Any misunderstanding can be avoided by explicitly noting that the convention of summation over repeated indices is *never* followed in this paper.

**3.2. Field point on the surface of the sphere $\alpha$.** When the field point $\mathbf{x}$ is taken on the surface of the sphere $\alpha$, we multiply (9) by $P_k^l(\cos\theta^\alpha)\cos l\psi^\alpha$ or $P_k^l(\cos\theta^\alpha)\sin l\psi^\alpha$ and integrate over the sphere's surface. The resulting equations are, respectively,

$$
\begin{aligned}
\frac{8\pi^2\epsilon_l(k+1)a^2}{(2k+1)^2}B_{kl}^\alpha = &-\int_{x_u}^{x_d}\Lambda_{kl}^\alpha(\mathbf{x}')\frac{r'\,dx'}{\cos\eta}\\
&-\int_0^{r_d}\Lambda_{kl}^\alpha(\mathbf{x}')\,r'dr'\\
&+4\pi a^2U\frac{a^k}{2k+1}\frac{(k+l)!}{(k-l)!}\int_{x_u}^{x_d}\tan\eta\,F_{Ckl}^{\alpha0}\,r'\,dx'\\
&+4\pi a^2\Delta U\frac{a^k}{2k+1}\frac{(k+l)!}{(k-l)!}\int_0^{r_d}F_{Ckl}^{\alpha0}\,r'\,dr'\\
&-\frac{4\pi v}{3}\left[(V_x^\alpha-U)\delta_{k,1}\delta_{l,0}-V_y^\alpha\delta_{k,1}\delta_{l,1}\right]\\
&-v\sum_{\beta=1,\beta\neq\alpha}^{N_S}\left\{\left[(V_x^\beta-U)G_{C10}^{kl}-2V_y^\beta G_{C11}^{kl}-2V_z^\beta\tilde{G}_{C11}^{kl}\right]\right\}\\
&+\sum_{\beta=1,\beta\neq\alpha}^{N_S}\sum_{n=1}^{\infty}\frac{4n\pi}{2n+1}a^{n+1}\sum_{m=0}^{n}\left(B_{nm}^\beta G_{Cnm}^{kl}+\tilde{B}_{nm}^\beta\tilde{G}_{Cnm}^{kl}\right)
\end{aligned}
\tag{24}
$$

and

$$
\begin{aligned}
\frac{8\pi^2(k+1)a^2}{(2k+1)^2}\tilde{B}_{kl}^\alpha = &-\int_{x_u}^{x_d}\tilde{\Lambda}_{kl}^\alpha(\mathbf{x}')\frac{r'\,dx'}{\cos\eta}\\
&-\int_0^{r_d}\tilde{\Lambda}_{kl}^\alpha(\mathbf{x}')\,r'dr'\\
&+4\pi a^2U\frac{a^k}{2k+1}\frac{(k+l)!}{(k-l)!}\int_{x_u}^{x_d}\tan\eta\,\tilde{F}_{Ckl}^{\alpha0}\,r'\,dx'\\
&+4\pi a^2\Delta U\frac{a^k}{2k+1}\frac{(k+l)!}{(k-l)!}\int_0^{r_d}\tilde{F}_{Ckl}^{\alpha0}\,r'\,dr'\\
&+\frac{4\pi v}{3}V_z^\alpha\delta_{k,1}\delta_{l,1}\\
&-v\sum_{\beta=1,\beta\neq\alpha}^{N_S}\left\{\left[(V_x^\beta-U)G_{S10}^{kl}-2V_y^\beta G_{S11}^{kl}-2V_z^\beta\tilde{G}_{S11}^{kl}\right]\right\}\\
&+\sum_{\beta=1,\beta\neq\alpha}^{N_S}\sum_{n=1}^{\infty}\frac{4n\pi}{2n+1}a^{n+1}\sum_{m=0}^{n}\left(B_{nm}^\beta G_{Snm}^{kl}+\tilde{B}_{nm}^\beta\tilde{G}_{Snm}^{kl}\right).
\end{aligned}
\tag{25}
$$

The functions $\Lambda_{kl}^\alpha(\mathbf{x}')$ and $\tilde{\Lambda}_{kl}^\alpha(\mathbf{x}')$ are defined by

$$
\Lambda_{kl}^\alpha(\mathbf{x}') = \int_0^{2\pi}\int_{S^\alpha}\phi(\mathbf{x}')\left(\frac{\partial}{\partial n'}\frac{1}{|\mathbf{x}-\mathbf{x}'|}\right)P_k^l(\cos\theta^\alpha)\cos l\psi^\alpha\,dS^\alpha(\mathbf{x})\,d\psi',
\tag{26}
$$

$$
\tilde{\Lambda}_{kl}^\alpha(\mathbf{x}') = \int_0^{2\pi}\int_{S^\alpha}\phi(\mathbf{x}')\left(\frac{\partial}{\partial n'}\frac{1}{|\mathbf{x}-\mathbf{x}'|}\right)P_k^l(\cos\theta^\alpha)\sin l\psi^\alpha\,dS^\alpha(\mathbf{x})\,d\psi',
\tag{27}
$$

in which

$$dS^\alpha(\mathbf{x}) = a^2 \sin\theta^\alpha \, d\theta^\alpha \, d\psi^\alpha.$$

After integration over $S^\alpha$, $\Lambda^\alpha_{kl}(\mathbf{x}')$ and $\tilde{\Lambda}^\alpha_{kl}(\mathbf{x}')$ become

$$\begin{aligned}
\Lambda^\alpha_{kl}(\mathbf{x}') &= \sum_{n=0}^{\infty} \frac{4\pi a^{k+2}}{2k+1} \frac{(k+l)!}{(k-l)!} \left( \Phi_n H^{\alpha n}_{Ckl} + \tilde{\Phi}_n H^{\alpha n}_{Skl} \right), \\
\tilde{\Lambda}^\alpha_{kl}(\mathbf{x}') &= \sum_{n=0}^{\infty} \frac{4\pi a^{k+2}}{2k+1} \frac{(k+l)!}{(k-l)!} \left( \Phi_n \tilde{H}^{\alpha n}_{Ckl} + \tilde{\Phi}_n \tilde{H}^{\alpha n}_{Skl} \right),
\end{aligned} \tag{28}$$

where the functions $H^{\alpha n}_{Ckl}$, $H^{\alpha n}_{Skl}$ are given by

$$H^{\alpha n}_{Ckl} = \frac{\partial}{\partial n'} F^{\alpha n}_{Ckl}, \qquad H^{\alpha n}_{Skl} = \frac{\partial}{\partial n'} F^{\alpha n}_{Skl}, \tag{29}$$

with the $F$'s as defined above and $\tilde{H}^{\alpha n}_{Ckl}$, $\tilde{H}^{\alpha n}_{Skl}$ given by similar expressions with the $F$'s replaced by $\tilde{F}$'s. With the definition $\mu = (x' - x^\alpha)/b$, in which $x^\alpha$ denotes the $x$-coordinate of the center of the sphere $\alpha$, the normal derivative of the spherical harmonics becomes

$$\frac{\partial}{\partial n'} \frac{P^m_n(\mu)}{b^{n+1}} = \mathbf{n}' \cdot \nabla \left[ \frac{P^m_n(\mu)}{b^{n+1}} \right],$$

where

$$\begin{aligned}
\nabla \left[ \frac{P^m_n(\mu)}{b^{n+1}} \right] &= -\mathbf{i} \frac{(n+m-1)P^m_{n+1}(\mu)}{b^{n+2}} \\
&\quad - \mathbf{j} \frac{\sqrt{1-\mu^2}[\mu(dP^m_n(\mu)/d\mu) + (n+1)P^m_n(\mu)]}{b^{n+2}}.
\end{aligned} \tag{30}$$

On the pipe, the normal vector becomes $\mathbf{n}' = -\mathbf{i}\sin\eta + \mathbf{j}\cos\eta$, while at the outlet $\mathbf{n}' = \mathbf{i}$.

The functions $G^{kl}_{Cnm}$, $\tilde{G}^{kl}_{Cnm}$, $G^{kl}_{Snm}$, and $\tilde{G}^{kl}_{Snm}$ are defined by

$$\begin{aligned}
G^{kl}_{Cnm} &= \int_{S^\alpha} \frac{Y^m_n(\Theta,\Psi)}{R^{n+1}} P^l_k(\cos\theta^\alpha) \cos l\psi^\alpha \, dS^\alpha(\mathbf{x}), \\
\tilde{G}^{kl}_{Cnm} &= \int_{S^\alpha} \frac{\tilde{Y}^m_n(\Theta,\Psi)}{R^{n+1}} P^l_k(\cos\theta^\alpha) \cos l\psi^\alpha \, dS^\alpha(\mathbf{x}), \\
G^{kl}_{Snm} &= \int_{S^\alpha} \frac{Y^m_n(\Theta,\Psi)}{R^{n+1}} P^l_k(\cos\theta^\alpha) \sin l\psi^\alpha \, dS^\alpha(\mathbf{x}), \\
\tilde{G}^{kl}_{Snm} &= \int_{S^\alpha} \frac{\tilde{Y}^m_n(\Theta,\Psi)}{R^{n+1}} P^l_k(\cos\theta^\alpha) \sin l\psi^\alpha \, dS^\alpha(\mathbf{x}),
\end{aligned} \tag{31}$$

where we use the definitions $\mathbf{x}^\alpha + \mathbf{y}^\alpha - \mathbf{x}^\beta = (R, \Theta, \Psi)$, with $\mathbf{x}^\alpha$ and $\mathbf{x}^\beta$ the position vectors of the centers of spheres $\alpha$ and $\beta$, while $\mathbf{y}^\alpha$ is the position vector from the center of the sphere $\alpha$ to the generic point on the surface of the same sphere. By using the relations (A.25) in the Appendix, the $G^{kl}_{Cnm}$, $\tilde{G}^{kl}_{Cnm}$, $G^{kl}_{Snm}$, and $\tilde{G}^{kl}_{Snm}$ can be calculated explicitly to find

$$\begin{aligned}
G^{kl}_{Cnm} &= D^{kl}_{nm}[C_A Y^{m+l}_{n+k}(\theta^{\alpha\beta}, \psi^{\alpha\beta}) + J^l_m C_B Y^{m-l}_{n+k}(\theta^{\alpha\beta}, \psi^{\alpha\beta})], \\
\tilde{G}^{kl}_{Cnm} &= D^{kl}_{nm}[C_A \tilde{Y}^{m+l}_{n+k}(\theta^{\alpha\beta}, \psi^{\alpha\beta}) + J^l_m C_B \tilde{Y}^{m-l}_{n+k}(\theta^{\alpha\beta}, \psi^{\alpha\beta})], \\
G^{kl}_{Snm} &= D^{kl}_{nm}[C_A \tilde{Y}^{m+l}_{n+k}(\theta^{\alpha\beta}, \psi^{\alpha\beta}) - J^l_m C_B \tilde{Y}^{m-l}_{n+k}(\theta^{\alpha\beta}, \psi^{\alpha\beta})], \\
\tilde{G}^{kl}_{Snm} &= D^{kl}_{nm}[-C_A Y^{m+l}_{n+k}(\theta^{\alpha\beta}, \psi^{\alpha\beta}) + J^l_m C_B Y^{m-l}_{n+k}(\theta^{\alpha\beta}, \psi^{\alpha\beta})],
\end{aligned} \tag{32}$$

in which $\mathbf{x}^\beta - \mathbf{x}^\alpha = (d^{\alpha\beta}, \theta^{\alpha\beta}, \psi^{\alpha\beta})$. The constants are

$$D_{nm}^{kl} = \frac{2\pi a^{k+2}(-1)^n}{(2k+1)(n+m)!(k-l)!}\frac{1}{(d^{\alpha\beta})^{k+n+1}}, \tag{33}$$

$$J_m^l = (-1)^{\min(l,m)}, \tag{34}$$

$$C_A = (n+k+m+l)!, \qquad C_B = (n+k+|m-l|)!. \tag{35}$$

When $m < l$, the proper definition of $\tilde{Y}_{n+k}^{m-l}$ is

$$\tilde{Y}_{n+k}^{m-l} = \frac{(n+k-|m-l|)!}{(n+k+|m-l|)!}P_{n+k}^{|m-l|}(\cos\theta^{\alpha\beta})\sin(m-l)\psi^{\alpha\beta}.$$

**3.3. Field point on the upstream and downstream sections.** On the pipe's cross sections $S_u$ and $S_d$, the value of the disturbance potential is taken to be uniform, zero in the first case, and given by (2) in the latter. In these cases, therefore, (4) must give the same result regardless of how the point $\mathbf{x}$ is chosen. This condition, of course, is only approximately true, and the extent to which it is verified may give a test of the accuracy of the calculation. In any case, the most convenient choice for the point $\mathbf{x}$ is now along the circle where the cross sections join the pipe's surface so that use can be made of (13) and (14) with $\gamma = \frac{1}{2}$.

Since on the upstream section $S_u$, for which $x = x_u$, $\phi = 0$, from (12) we find that $\Phi_j = \tilde{\Phi}_j = 0$ for $j = 0, 1, 2, \ldots$; (9) gives

$$\begin{aligned}
0 = &-\int_{x_u}^{x_d}\Psi_l(x_u,x',t)\frac{r'\,dx'}{\cos\eta} - \int_0^{r_d}\Psi_l(x_u,x',t)r'\,dr' \\
&+ 4\pi U\epsilon_l\delta_{l,0}\int_{x_u}^{x_d}\tan\eta\frac{K(m)}{A^{1/2}}r'\,dx' \\
&+ 4\pi\Delta U\epsilon_l\delta_{l,0}\int_0^{r_d}\frac{K(m)}{A^{1/2}}r'\,dr' \\
&- v\sum_{\alpha=1}^{N_S}\left[\left\{(V_x^\alpha - U)F_{C10}^l - 2V_y^\alpha F_{C11}^l - 2V_z^\alpha\tilde{F}_{C11}^l\right\}\right] \\
&+ \sum_{\alpha=1}^{N_S}\sum_{n=1}^{\infty}\frac{4n\pi}{2n+1}a^{n+1}\sum_{m=0}^{n}\left\{B_{nm}^\alpha F_{Cnm}^l + \tilde{B}_{nm}^\alpha\tilde{F}_{Cnm}^l\right\}
\end{aligned} \tag{36}$$

and

$$\begin{aligned}
0 = &-\int_{x_u}^{x_d}\tilde{\Psi}_l(x_u,x',t)\frac{r'\,dx'}{\cos\eta} - \int_0^{r_d}\tilde{\Psi}_l(x_u,x',t)r'\,dr' \\
&- v\sum_{\alpha=1}^{N_S}\left[\left\{(V_x^\alpha - U)F_{S10}^l - 2V_y^\alpha F_{S11}^l - 2V_z^\alpha\tilde{F}_{S11}^l\right\}\right] \\
&+ \sum_{\alpha=1}^{N_S}\sum_{n=1}^{\infty}\frac{4n\pi}{2n+1}a^{n+1}\sum_{m=0}^{n}\left\{B_{nm}^\alpha F_{Snm}^l + \tilde{B}_{nm}^\alpha\tilde{F}_{Snm}^l\right\}.
\end{aligned} \tag{37}$$

Similarly, for $\mathbf{x}$ on the circle at which $S_d$ joins the pipe's surface, $x = x_d$, and

$$
\begin{aligned}
\pi^2\epsilon_l\Phi_l(x_d) = &-\int_{x_u}^{x_d}\Psi_l(x_d,x',t)\frac{r'\,dx'}{\cos\eta}-\int_0^{r_d}\Psi_l(x_d,x',t)r'\,dr' \\
&+4\pi U\epsilon_l\delta_{l,0}\int_{x_u}^{x_d}\tan\eta\frac{K(m)}{A^{1/2}}r'\,dx' \\
&+4\pi\Delta U\epsilon_l\delta_{l,0}\int_0^{r_d}\frac{K(m)}{A^{1/2}}r'\,dr' \\
&-v\sum_{\alpha=1}^{N_S}\left[\left\{(V_x^\alpha-U)F_{C10}^l-2V_y^\alpha F_{C11}^l-2V_z^\alpha\tilde{F}_{C11}^l\right\}\right] \\
&+\sum_{\alpha=1}^{N_S}\sum_{n=1}^{\infty}\frac{4n\pi}{2n+1}a^{n+1}\sum_{m=0}^{n}\left\{B_{nm}^\alpha F_{Cnm}^l+\tilde{B}_{nm}^\alpha\tilde{F}_{Cnm}^l\right\}
\end{aligned}
\tag{38}
$$

and

$$
\begin{aligned}
\pi^2\tilde{\Phi}_l(x_d) = &-\int_{x_u}^{x_d}\tilde{\Psi}_l(x_d,x',t)\frac{r'\,dx'}{\cos\eta}-\int_0^{r_d}\tilde{\Psi}_l(x_d,x',t)r'\,dr' \\
&-v\sum_{\alpha=1}^{N_S}\left[\left\{(V_x^\alpha-U)F_{S10}^l-2V_y^\alpha F_{S11}^l-2V_z^\alpha\tilde{F}_{S11}^l\right\}\right] \\
&+\sum_{\alpha=1}^{N_S}\sum_{n=1}^{\infty}\frac{4n\pi}{2n+1}a^{n+1}\sum_{m=0}^{n}\left\{B_{nm}^\alpha F_{Snm}^l+\tilde{B}_{nm}^\alpha\tilde{F}_{Snm}^l\right\}.
\end{aligned}
\tag{39}
$$

According to (2), at $x = x_d$, $\Phi_0 = C + \Delta U\, x_d$ while all other $\Phi_l$ and $\tilde{\Phi}_l$ vanish. Hence, of all the equations given in this subsection, the only one that is needed for the solution of the problem is (38), written for $l = 0$, from which $C$ can be determined. All the other relations must hold automatically, at least approximately, if the assumptions made are consistent and the numerical algorithm correct.

**4. Equations of motion.** Since the spheres are taken to be massless, the total force on each one of them must vanish, so that

$$
0 = \int_{S^\alpha} p\mathbf{n}dS^\alpha = -\rho\int_{S^\alpha}\left[\frac{\partial\phi_T}{\partial t}+\frac{1}{2}(\nabla\phi_T)^2+gx\right]\mathbf{n}\,dS^\alpha,
\tag{40}
$$

where the unit normal vector $\mathbf{n}$ is, in the local spherical coordinate system,

$$
\mathbf{n} = \mathbf{i}\cos\theta^\alpha+\mathbf{j}\sin\theta^\alpha\cos\psi^\alpha+\mathbf{k}\sin\theta^\alpha\sin\psi^\alpha,
$$

and the gravity force has been taken to act in the direction parallel to the axis of the pipe. Since, on the surface of the sphere $\alpha$, $\phi_T$ is given by

$$
\phi_T = U(t)x+\phi^\alpha,
\tag{41}
$$

the quantity in brackets in (40) becomes

$$
\frac{D\phi^\alpha}{Dt}+\frac{dU}{dt}x-V_x^\alpha U+\frac{U^2}{2}-(\mathbf{V}^\alpha-\mathbf{i}U)\cdot\nabla\phi^\alpha+\frac{1}{2}(\nabla\phi^\alpha)^2+gx.
\tag{42}
$$

Here we have denoted by $D\phi^\alpha/Dt$ the derivative of (10) with respect to the variable $t$ explicitly appearing there as argument of $B_{nm}^\alpha$, $\tilde{B}_{nm}^\alpha$. Furthermore, for (42) to be strictly correct, we must interpret $\nabla\phi^\alpha$ as

$$
\nabla\phi^\alpha = (\mathbf{V}^\alpha\cdot\mathbf{n})\,\mathbf{n}+\frac{1}{a}\frac{\partial\phi^\alpha}{\partial\theta^\alpha}+\frac{1}{a\sin\theta^\alpha}\frac{\partial\phi^\alpha}{\partial\psi^\alpha}.
\tag{43}
$$

The first term, however, contributes nothing to the integral in (40), so that the abbreviated notation adopted in (42) is justified in spite of the slightly inconsistency.

Substitution of (42) into (40) and integration by means of the known properties of the associated Legendre functions gives equations of motion for each direction. For the $x$-direction, (40) leads to

$$\begin{aligned}&\frac{dB_{10}^{\alpha}}{dt}+a\frac{dU}{dt}-\frac{6}{5}\frac{1}{a}(V_x^{\alpha}-U)B_{20}^{\alpha}+\frac{3}{10}\frac{1}{a}(V_y^{\alpha}B_{21}^{\alpha}+V_z^{\alpha}\tilde{B}_{21}^{\alpha})\\&\quad+\frac{3}{a^2}\sum_{n=1}^{\infty}\frac{n(n+1)(n+2)}{(2n+1)(2n+3)}B_{n0}^{\alpha}B_{n+1,0}^{\alpha}\\&\quad+\frac{3}{2}\frac{1}{a^2}\sum_{n=1}^{\infty}\sum_{m=1}^{n}C_n\frac{(n-m+1)!}{(n+m)!}(B_{nm}^{\alpha}B_{n+1,m}^{\alpha}+\tilde{B}_{nm}^{\alpha}\tilde{B}_{n+1,m}^{\alpha})\\&\quad+ag=0,\end{aligned}\tag{44}$$

while, for the $y$-direction,

$$\begin{aligned}&-\frac{dB_{11}^{\alpha}}{dt}+\frac{3}{5}\frac{1}{a}(V_x^{\alpha}-U)B_{21}^{\alpha}+\frac{6}{5}\frac{1}{a}V_y^{\alpha}B_{20}^{\alpha}-\frac{3}{10}\frac{1}{a}(V_y^{\alpha}B_{22}^{\alpha}+V_z^{\alpha}\tilde{B}_{22}^{\alpha})\\&\quad+\frac{3}{a^2}\sum_{n=1}^{\infty}C_n(B_{n+1,0}^{\alpha}B_{n1}^{\alpha}-B_{n+1,1}^{\alpha}B_{n0}^{\alpha})\\&\quad+\frac{3}{2a^2}\sum_{n=1}^{\infty}\sum_{m=1}^{n-1}C_n\frac{(n-m+1)!}{(n+m+1)!}(B_{n+1,m}^{\alpha}B_{n,m+1}^{\alpha}+\tilde{B}_{n+1,m}^{\alpha}\tilde{B}_{n,m+1}^{\alpha})\\&\quad-\frac{3}{2a^2}\sum_{n=1}^{\infty}\sum_{m=1}^{n}C_n\frac{(n-m)!}{(n+m)!}(B_{nm}^{\alpha}B_{n+1,m+1}^{\alpha}+\tilde{B}_{nm}^{\alpha}\tilde{B}_{n+1,m+1}^{\alpha})=0,\end{aligned}\tag{45}$$

and, for the $z$-direction,

$$\begin{aligned}&-\frac{d\tilde{B}_{11}^{\alpha}}{dt}+\frac{3}{5}\frac{1}{a}(V_x^{\alpha}-U)\tilde{B}_{21}^{\alpha}+\frac{6}{5}\frac{1}{a}V_z^{\alpha}B_{20}^{\alpha}-\frac{3}{10}\frac{1}{a}(V_y^{\alpha}\tilde{B}_{22}^{\alpha}-V_z^{\alpha}B_{22}^{\alpha})\\&\quad+\frac{3}{a^2}\sum_{n=1}^{\infty}C_n(B_{n+1,0}^{\alpha}\tilde{B}_{n1}^{\alpha}-\tilde{B}_{n+1,1}^{\alpha}B_{n0}^{\alpha})\\&\quad+\frac{3}{2a^2}\sum_{n=1}^{\infty}\sum_{m=1}^{n-1}C_n\frac{(n-m+1)!}{(n+m+1)!}(B_{n+1,m}^{\alpha}\tilde{B}_{n,m+1}^{\alpha}-\tilde{B}_{n+1,m}^{\alpha}B_{n,m+1}^{\alpha})\\&\quad-\frac{3}{2a^2}\sum_{n=1}^{\infty}\sum_{m=1}^{n}C_n\frac{(n-m)!}{(n+m)!}(B_{nm}^{\alpha}\tilde{B}_{n+1,m+1}^{\alpha}-\tilde{B}_{nm}^{\alpha}B_{n+1,m+1}^{\alpha})=0,\end{aligned}\tag{46}$$

where

$$C_n=\frac{n(n+2)}{(2n+1)(2n+3)}.$$

Finally, the position of the center of the sphere is related to its velocity by

$$\frac{d\mathbf{x}^{\alpha}}{dt}=\mathbf{V}^{\alpha}.\tag{47}$$

**5. Axisymmetric case.** When the spheres are constrained to remain on the axis of the pipe, due to the axial symmetry of the configuration, a considerable simplification of the above formulae occurs. The potential on the surface of the sphere $\alpha$, (10), can be written as

$$\phi^\alpha = \sum_{n=1}^{\infty} B^\alpha_{n,0} P_n(\cos\theta^\alpha), \tag{48}$$

while the potential on the surface of the pipe (12) becomes

$$\phi(\mathbf{x},t) = \Phi_0(x,t).$$

Equation (13) then becomes

$$\begin{aligned}\gamma\Phi_0(x) = {} & \frac{2}{\pi}\int_{x_u}^{x_d} \frac{B^0(x,x',r,r')}{A^{3/2}}\Phi_0(x')\frac{r'\,dx'}{\cos\eta} \\ & + \frac{2}{\pi}\int_0^{r_d} \frac{(x_d-x)}{A^{3/2}}\Phi_0(x')\frac{E(m)}{1-m}r'\,dr \\ & + \frac{2U}{\pi}\int_{x_u}^{x_d} \tan\eta\frac{K(m)}{A^{1/2}}r'\,dx' \\ & + \frac{2\Delta U}{\pi}\int_0^{r_d} \frac{K(m)}{A^{1/2}}r'\,dr' \\ & - \frac{2}{3}\left(\frac{a}{R}\right)^2 a\sum_{\alpha=1}^{N_S}(V_x^\alpha - U)P_1(\cos\theta^\alpha) \\ & + \sum_{\alpha=1}^{N_S}\sum_{n=1}^{\infty}\frac{2n}{2n+1}\left(\frac{a}{R}\right)^{n+1} B^\alpha_{n,0}P_n(\cos\theta^\alpha).\end{aligned} \tag{49}$$

In (32) the only nonzero term is

$$G^{k,0}_{Cn0} = 2(n+k)!D^{k,0}_{n,0}P_{k+n}(\cos\theta^{\alpha\beta}),$$

in which $\theta^{\alpha\beta} = 0$ if $x^\beta > x^\alpha$, while $\theta^{\alpha\beta} = \pi$ if $x^\beta < x^\alpha$. Equation (24) then becomes

$$\begin{aligned}B^\alpha_{k,0} = {} & -\frac{2k+1}{2(k+1)}a^k\int_{x_u}^{x_d}\Phi_0(x')\frac{\partial}{\partial n'}\frac{P_k(\cos\theta^\alpha)}{R^{k+1}}\frac{r'\,dx'}{\cos\eta} \\ & + \frac{2k+1}{2}a^k\int_0^{r_d}\Phi_0(x_d)\frac{P_{k+1}(\cos\theta^\alpha)}{R^{k+2}}r'\,dr' \\ & + \frac{2k+1}{2(k+1)}a^k U\int_{x_u}^{x_d}\tan\eta\frac{P_k(\cos\theta^\alpha)}{R^{k+1}}r'\,dx' \\ & + \frac{2k+1}{2(k+1)}\Delta U a^k\int_0^{r_d}\frac{P_k(\cos\theta^\alpha)}{R^{k+1}}r'\,dr' \\ & - \frac{1}{2}a(V_x^\alpha - U)\delta_{k,1} - \frac{2k+1}{3}\sum_{\beta=1,\beta\neq\alpha}^{N_S} S^1_k a(V_x^\beta - U)\left(\frac{a}{d^{\alpha\beta}}\right)^{k+2} \\ & + \frac{2k+1}{k+1}\sum_{\beta=1,\beta\neq\alpha}^{N_S}\sum_{n=1}^{\infty}\frac{n}{2n+1}\frac{(n+k)!}{n!k!}S^n_k\left(\frac{a}{d^{\alpha\beta}}\right)^{k+n+1}B^\beta_{n,0},\end{aligned} \tag{50}$$

where

$$S_k^n = (-1)^n \quad \text{if } x^\beta > x^\alpha, \qquad S_k^n = (-1)^k \quad \text{if } x^\beta < x^\alpha.$$

The equation of motion (44) becomes

$$\begin{aligned} &\frac{dB_{10}^\alpha}{dt} + a\frac{dU}{dt} - \frac{6}{5}\frac{1}{a}(V_x^\alpha - U)B_{20}^\alpha \\ &\quad + \frac{3}{a^2}\sum_{n=1}^{\infty}\frac{n(n+1)(n+2)}{(2n+1)(2n+3)}B_{n,0}^\alpha B_{n+1,0}^\alpha + ag = 0. \end{aligned} \tag{51}$$

In the simple case of a single sphere moving through an unbounded liquid, it can be shown from (50) that

$$B_{10} = -\tfrac{1}{2}a\,(V - U), \tag{52}$$

while all the other coefficients vanish. In this case, with the neglect of gravity, the equation of motion (51) reduces to the familiar result

$$\frac{dV}{dt} = 3\frac{dU}{dt}. \tag{53}$$

**6. Spheres in an unbounded liquid.** Another limit case of interest contained in the formulation of §§2 and 3 is that in which the spheres are immersed in an unbounded liquid at rest at infinity. In this case, the term $Ux$ in expression (1) of the velocity potential vanishes and only the disturbance potential remains. By neglecting the contribution of the pipe's surface and the upstream and downstream surfaces $S_u$, $S_d$ in (24) and (25), we find that

$$\begin{aligned} \epsilon_l B_{kl}^\alpha = &-aV_x^\alpha \delta_{k,1}\delta_{l,0} + aV_y^\alpha \delta_{k,1}\delta_{l,1} \\ &-a\sum_{\beta=1,\beta\neq\alpha}^{N_S}\left[V_x^\beta Q_{C10}^{kl} - 2V_y^\beta Q_{C11}^{kl} - 2V_z^\beta \tilde{Q}_{C11}^{kl}\right]\lambda^{k+2} \\ &+\sum_{\beta=1,\beta\neq\alpha}^{N_S}\sum_{n=1}^{\infty}\sum_{m=0}^{n}\left[B_{nm}^\beta Q_{Cnm}^{kl} + \tilde{B}_{nm}^\beta \tilde{Q}_{Cnm}^{kl}\right]\lambda^{k+n+1} \end{aligned} \tag{54}$$

and

$$\begin{aligned} \tilde{B}_{kl}^\alpha = &aV_z^\alpha \delta_{k,1}\delta_{l,1} \\ &-a\sum_{\beta=1,\beta\neq\alpha}^{N_S}\left[V_x^\beta Q_{S10}^{kl} - 2V_y^\beta Q_{S11}^{kl} - 2V_z^\beta \tilde{Q}_{S11}^{kl}\right]\lambda^{k+2} \\ &+\sum_{\beta=1,\beta\neq\alpha}^{N_S}\sum_{n=1}^{\infty}\sum_{m=0}^{n}\left[B_{nm}^\beta Q_{Snm}^{kl} + \tilde{B}_{nm}^\beta \tilde{Q}_{Snm}^{kl}\right]\lambda^{k+n+1}, \end{aligned} \tag{55}$$

in which

$$\lambda = \frac{a}{d^{\alpha\beta}}, \tag{56}$$

and the new coefficients $Q_{Cnm}^{kl}$ are defined by

$$Q_{Cnm}^{kl} = \frac{(2k+1)^2 n a^{n-1}}{2\pi(k+1)(2n+1)}G_{Cnm}^{kl},$$

with similar relations for $Q^{kl}_{Snm}$, $\tilde{Q}^{kl}_{Cnm}$, and $\tilde{Q}^{kl}_{Snm}$. The equations of motion (44)–(46) still hold, except that $U = 0$, $\Delta U = 0$ in this case.

It may be noted that these equations can be derived alternatively by using a Lagrangian. The kinetic energy of an unbounded liquid at rest at infinity in which $N_S$ spheres are in motion is given by

$$T = -\frac{\rho}{2}\sum_{\alpha=1}^{N_S}\int_{S^\alpha}\phi^\alpha\frac{\partial\phi^\alpha}{\partial n}dS^\alpha. \tag{57}$$

Carrying out the integration over the surface of the spheres yields

$$T = \frac{\rho v}{2a}\sum_{\alpha=1}^{N_S}\left[-B^\alpha_{10}V^\alpha_x + \frac{1}{2}B^\alpha_{11}V^\alpha_y + \frac{1}{2}\tilde{B}^\alpha_{11}V^\alpha_z\right], \tag{58}$$

where, as before, $v$ denotes the volume of the spheres. The equations of motion are derived from

$$\frac{d}{dt}\left\{\frac{\partial T}{\partial\dot{q}_i}\right\} - \frac{\partial T}{\partial q_i} = f_i, \tag{59}$$

where the generalized coordinates are

$$q_i = x^\alpha,\ y^\alpha,\ z^\alpha, \quad \alpha = 1,\ldots,N_S,$$

and $f_i$ denotes the force acting on the sphere in the direction of the coordinate $q_i$. It might seem that this Lagrangian approach might be easier to implement than the method described in the previous section because only the $B^\alpha_{10}$, $B^\alpha_{11}$, and $\tilde{B}^\alpha_{11}$ in (58) would be required. However, these quantities depend on the velocity and positions of the spheres through (54) and (55), and a derivation of the explicit expression of this dependence is far from trivial.

An approximate solution of these equations can, however, be found if the spheres are well separated from each other so that $\lambda << 1$. In this case, we find approximately that

$$2B^\alpha_{10} = -aV^\alpha_x + \sum_{\beta=1,\beta\neq\alpha}^{N_S}\left[-\frac{3}{2}aV^\beta_xQ^{10}_{C10} + 3aV^\beta_yQ^{10}_{C11} + 3aV^\beta_z\tilde{Q}^{10}_{C11}\right]\lambda^3 + O(\lambda^6), \tag{60}$$

$$B^\alpha_{11} = aV^\alpha_y + \sum_{\beta=1,\beta\neq\alpha}^{N_S}\left[-\frac{3}{2}aV^\beta_xQ^{11}_{C10} + 3aV^\beta_yQ^{11}_{C11} + 3aV^\beta_z\tilde{Q}^{11}_{C11}\right]\lambda^3 + O(\lambda^6), \tag{61}$$

$$\tilde{B}^\alpha_{11} = aV^\alpha_z + \sum_{\beta=1,\beta\neq\alpha}^{N_S}\left[-\frac{3}{2}aV^\beta_xQ^{11}_{S10} + 3aV^\beta_yQ^{11}_{S11} + 3aV^\beta_z\tilde{Q}^{11}_{S11}\right]\lambda^3 + O(\lambda^6). \tag{62}$$

Let us consider the special case of two spheres. It is convenient to take the $x$-axis in the direction joining the centers so that $|x^\beta - x^\alpha| = d$. If the two spheres are

moving along the $x$-axis (i.e., along the line joining their centers), these relations give

$$B_{10}^{\alpha} = -\frac{aV_x^{\alpha}}{2} + \frac{3}{2}aV_x^{\beta}\lambda^3 + O(\lambda^6),$$
$$B_{10}^{\beta} = -\frac{aV_x^{\beta}}{2} + \frac{3}{2}aV_x^{\alpha}\lambda^3 + O(\lambda^6), \tag{63}$$

while the other $B$'s vanish. If the two spheres are moving in a direction perpendicular to the $x$-axis, we find that

$$B_{11}^{\alpha} = aV_y^{\alpha} + \tfrac{3}{2}aV_y^{\beta}\lambda^3 + O(\lambda^6),$$
$$B_{11}^{\beta} = aV_y^{\beta} + \tfrac{3}{2}aV_y^{\alpha}\lambda^3 + O(\lambda^6), \tag{64}$$

with all the other $B$'s vanishing as before. These results coincide with the expressions given by Milne-Thomson [25].

Another case in which the dependence of the $B$'s on velocity and positions of the spheres can be found explicitly—and, in this case, exactly—is the case in which only two spheres are present. This was essentially done by van Wijngaarden [36] by a procedure different from the one used here (see also Kok [24]). For more than two spheres, or in the presence of boundaries, it does not seem likely that (24) and (25) can be solved explicitly.

**7. Numerical implementation.** The first step in rendering numerically tractable the formulation derived in the previous sections consists in truncating the infinite series. Thus we use a finite number $N_F$ of terms in the Fourier series of the potential on the pipe's wall and truncate the multipole expansion (10) of the potential on the surface of the $\alpha$th sphere to $M^{\alpha}$ terms. For efficiency, this quantity can be adjusted in the course of the computation by monitoring the magnitude of the coefficients $B^{\alpha}$.

A discretization of the integrals along the axis of the pipe occurring in many of the preceding formulae must also be carried out. For this purpose, we subdivide the region $x_u \le x \le x_d$ into $N_w$ intervals so that

$$\int_{x_u}^{x_d} \cong \sum_{j=0}^{N_w} \int_{x_j}^{x_{j+1}}$$

with $x_0 = x_u$, $x_{N_w+1} = x_d$. We take the Fourier coefficients of the potential on the pipe's surface $\Phi(x,t)$ and $\tilde{\Phi}(x,t)$ to be linear functions of $x$ between the two nodal values $\Phi(x_j,t)$ and $\Phi(x_{j+1},t)$. More refined numerical treatments of this part of the problem can readily be introduced. Equations (13) and (14) are then written at the points $x_j$, $j = 1, 2, \ldots, N_w$. At $x_0 = x_u$, we use (36) and (37), and at $x_{N_w+1} = x_d$ we use (38) and (39). For all the segments over which the integrands are regular, the integration is carried out by means of a standard ten-point Gaussian formula. However, due to the presence of the elliptic integrals, some integrands become logarithmically singular when $x = x'$. These singular integrations are carried out by use of a ten-point Gaussian formula with a logarithmic weight.

The complete solution of the problem also requires the time integration of (40) and (47) and the determination of $B^{\alpha}$, $\tilde{B}^{\alpha}$. These steps are carried out by a predictor-corrector method as follows:

(a) Suppose that at the generic time $t_k$ the values of all variables are known;

(b) At time $t_{k+1} = t_k + \Delta t$, determine low-accuracy approximations of $B_{10}^{\alpha}(t_{k+1})$, $B_{11}^{\alpha}(t_{k+1})$, and $\tilde{B}_{11}^{\alpha}(t_{k+1})$ by an explicit first-order Euler step from (44)–(46). For example, $B_{10}^{\alpha}(t_{k+1})$ is estimated according to

$$B_{10}^{\alpha}(t_{k+1}) = B_{10}^{\alpha}(t_k) + \Delta t F_x(t_k), \tag{65}$$

where $F_x(t_k)$ stands for all the nonlinear and gravity terms in (44);

(c) By using these estimates of $B_{10}^{\alpha}(t_{k+1})$, $B_{11}^{\alpha}(t_{k+1})$, and $\tilde{B}_{11}^{\alpha}(t_{k+1})$, calculate corresponding estimates for $\mathbf{V}^{\alpha}(t_{k+1})$, $\Phi_n(t_{k+1})$, $\tilde{\Phi}_n(t_{k+1})$, and the rest of the coefficients of $B_{nm}^{\alpha}(t_{k+1})$ and $\tilde{B}_{nm}^{\alpha}(t_{k+1})$ from (13), (14), (24), and (25);

(d) Determine new values for the positions $\mathbf{x}^{\alpha}(t_{k+1})$ of the spheres' centers from the new velocities $\mathbf{V}^{\alpha}(t_{k+1})$, according to

$$\mathbf{x}^{\alpha}(t_{k+1}) = \mathbf{x}^{\alpha}(t_k) + \frac{\Delta t}{2}[\mathbf{V}^{\alpha}(t_{k+1}) + \mathbf{V}^{\alpha}(t_k)]; \tag{66}$$

(e) Update the coefficients of all the equations by using the new values for the locations $\mathbf{x}^{\alpha}(t_{k+1})$ of the centers;

(f) Obtain improved estimates of $B_{10}^{\alpha}(t_{k+1})$, $B_{11}^{\alpha}(t_{k+1})$, and $\tilde{B}_{11}^{\alpha}(t_{k+1})$ by using the same method used in step (d);

(g) Go back to step (c) and repeat the cycle until suitable convergence criteria are met.

Note that in (50) the interaction between two spheres $\alpha$ and $\beta$ is $O((a/d^{\alpha\beta})^3)$, where $d^{\alpha\beta}$ is the distance between their centers. Therefore, for spheres well separated from each other and also from the pipe's wall, the above iteration converges very quickly.

**8. Some numerical examples.** In the examples described in this section, use is made of dimensionless variables defined in terms of the common radius $a$ of the spheres and a characteristic velocity $U_c$ as

$$\begin{aligned} x^* &= x/a, \qquad t^* = U_c\, t/a, \\ U^* &= U/U_c, \qquad \phi^{\alpha *} = \phi^{\alpha}/aU_c. \end{aligned} \tag{67}$$

For motion under the action of the external field $g$, the characteristic velocity $U_c$ is taken as $U_c = \sqrt{ag}$, while, in the absence of the external field, we take $U_c$ equal to the volume velocity at the upstream section $S_u$. In the remainder of this section, only dimensionless variables are used, but the asterisks are omitted for convenience.

In all the examples to be considered, the upstream volumetric flow rate $\pi S_u U$ is taken to be independent of time. Furthermore, the initial velocity of the spheres is always taken to be parallel and equal to that of the liquid.

In setting up the complex calculation described above, a major concern is, of course, the validation of the method and of its numerical implementation. This point is not trivial because no exact analytic solutions exist with which to compare the results. The few available analytic results are only applicable to weakly interacting spheres and therefore do not constitute a stringent test of the approach. We have therefore used comparisons with other numerical calculations and fundamental conservation and invariance principles that are known to hold exactly.

Our first test was for the case of the flow of a pure liquid without any sphere. For this case, we took an axisymmetric nozzle with a profile given by

$$\begin{aligned} &r = r_u, && -18 < x < -6, \\ &r = r_u - (r_u - r_m)\cos^2\left[\frac{\pi}{8}(x+2)\right], && -6 < x < -2, \\ &r = r_m, && -2 < x < 0 \end{aligned} \tag{68}$$

with $r_u = r_d = 4$, $r_m = 2\sqrt{2}$. The nozzle is symmetric with respect to $x = 0$. It was discretized by placing nodes at intervals $\Delta x = r(x)/8$, where $r(x)$ is the radius of the local cross section. This resulted in a total of 73 nodes. We have compared our

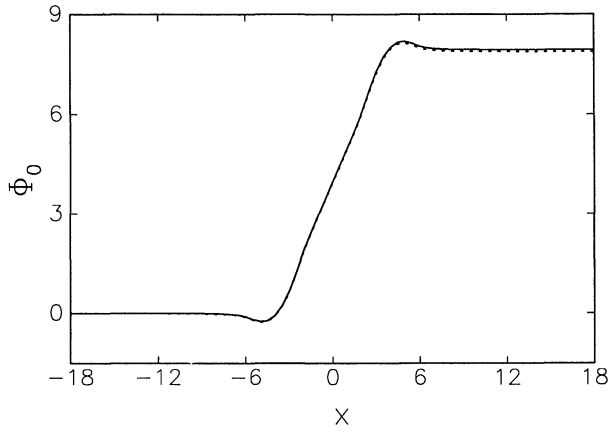


FIG. 3. *Comparison between two numerical results for the value of the potential on the surface of a pipe with variable cross section given by* (68). *Solid line: present calculation; dashed line: Dr. Oğuz's code.*

results with those given by an independent potential flow code kindly made available to us by Dr. Hasan N. Oğuz. Figure 3 shows a comparison of the two results for the wall values of the potential along the pipe. The solid line is our calculation and the dashed line Dr. Oğuz's. We have found that agreement between the two results could be improved further by refining the discretizations used in the two codes, and we are therefore satisfied that the two calculations agree with each other.

Another way to test the accuracy of the calculation is to monitor conservation of the total energy $\mathcal{E}$. With no gravity the energy is purely kinetic and, with $S_u = S_d$, its dimensionless value $\mathcal{K}$ is given by

$$\mathcal{K} = \frac{\pi}{2} r_d^2 \left[ (x_d - x_u) U^2 + C(t)\, U \right] + \frac{2\pi}{3} \sum_{\alpha=1}^{N_S} \left[ (U + B_{10}^{\alpha}) V_x^{\alpha} - \frac{1}{2} B_{11}^{\alpha} V_y^{\alpha} - \frac{1}{2} \tilde{B}_{11}^{\alpha} V_z^{\alpha} \right]. \tag{69}$$

Here and in the following, the energy is nondimensionalized by dividing by $\rho a^3 U_c^2$, where $\rho$ is the liquid density. The first term in this equation is of the order of the total kinetic energy of the liquid in the absence of the spheres and is therefore usually much larger than the second one. A consideration of the total kinetic energy would thus be a rather insensitive test of the accuracy of the calculation. Hence, we subtract out the (constant) dominant term and examine the conservation of

$$\mathcal{K}' = \frac{\pi}{2} r_d^2\, C(t)\, U + \frac{2\pi}{3} \sum_{\alpha=1}^{N_S} \left[ (U + B_{10}^{\alpha}) V_x^{\alpha} - \frac{1}{2} B_{11}^{\alpha} V_y^{\alpha} - \frac{1}{2} \tilde{B}_{11}^{\alpha} V_z^{\alpha} \right]. \tag{70}$$

In terms of this quantity, a useful measure of the error is

$$\text{error} = \frac{\mathcal{K}'(t) - \mathcal{K}'(0)}{\mathcal{K}'(0)}. \tag{71}$$

For our first test, we take an axisymmetric problem with a single sphere placed on the axis of a nozzle with the same shape (68) used for the previous example, but

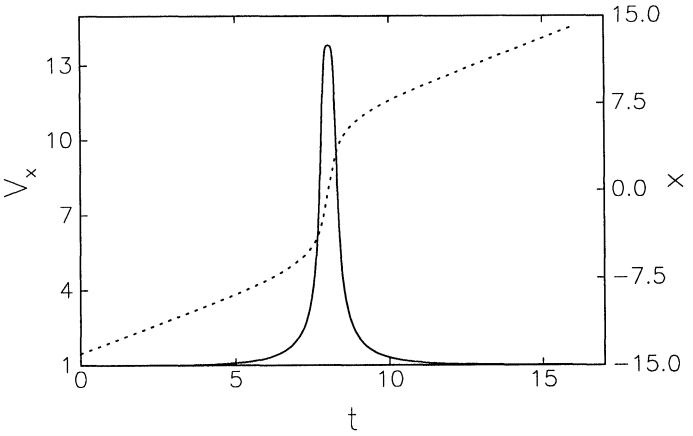


FIG. 4. *Velocity (solid line, left vertical scale) and position (dotted line, right vertical scale) of a single sphere convected along the axis of the nozzle* (68) *with a minimum radius* $r_m = 1.2$.

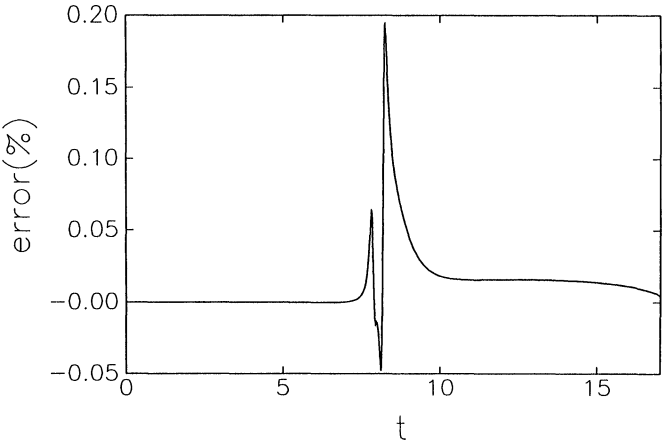


FIG. 5. *Energy error* (71) *versus time for the sphere in a nozzle of the previous figure.*

with a much narrower throat, $r_m = 1.2$. Initially, the sphere is at $x = -14$, and it has the same velocity as the liquid, $U = 1$. For this calculation as well as all the other ones described below, the pipe wall was discretized with 37 points. This number was arrived at using the rule $\Delta x = \frac{1}{4}r(x)$ for this case with $r_m = 1.2$, but the number of points was not changed for other values of $r_m$. The ratio $B^1_{N0}/B^1_{10}$ of the last coefficient retained to the first one was constrained to remain between $10^{-5}$ and $10^{-3}$ by adding or deleting terms in the Legendre expansion (48). The minimum value of $N$ was prescribed to be 5, and the maximum value reached during the calculation was 18. Figure 4 shows, as a function of time, the velocity of the sphere (solid line, left vertical scale) and its position (dotted line, right vertical scale). Figure 5 is a graph of the error, defined by (71), as a function of time. It can be seen that the maximum is of the order of 0.2 percent.

Another energy conservation test was conducted for the case of a liquid quiescent except for the motion induced by a gravity field acting along the pipe's axis. In this

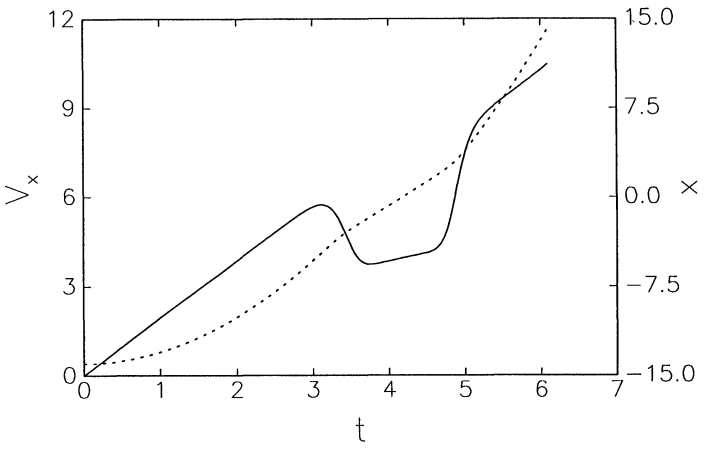


FIG. 6. *Velocity (solid line, left vertical scale) and position (dotted line, right vertical scale) of a buoyant sphere rising along the axis of the nozzle* (68) *with a minimum radius* $r_m = 1.2$ *sphere radii. The liquid is at rest except for the motion of the sphere.*

case, the total energy is given by

$$\mathcal{E} = \mathcal{K} + \frac{4}{3}\pi \sum_{\alpha=1}^{N_S} x^\alpha. \tag{72}$$

We simulated the same single-sphere problem mentioned before for this case. For this calculation and the other axisymmetric ones described below, the number of coefficients retained in expansion (48) was kept fixed at 12. The velocity and position versus time are shown in Fig. 6 and the energy error in Fig. 7. In this case, the latter is defined by

$$\text{error} = \frac{\mathcal{E}(t) - \mathcal{E}(0)}{\mathcal{E}(0)} \tag{73}$$

and reaches a maximum of the order of 2 percent. This value is one order of magnitude greater than before, which is only partially a consequence of the fewer terms retained in expansion (48). A circumstance of greater importance is the fact that $C(t)$ in (69) or (70) is typically greater than the terms in the summation, so that definition (73) used in this case is more sensitive to numerical error than the previous one (71).

Figure 8 shows velocities and positions as a function of time for two spheres convected along the axis of the same nozzle (68) with a minimum radius $r_m = 1.5$. Initially, the spheres' centers are separated by 2.2 units, so that the distance between the closest points on their surfaces is 20 percent of the radius. The maximum error in this case was 0.1 percent. Figure 9 is for the same nozzle and initial configuration of two spheres, but this time the motion is driven by a gravitational field directed along the pipe's axis.

We now consider a few simple nonaxisymmetric examples. For the first one, we initially place a single sphere, having the same velocity as the liquid, with its center at one unit from the pipe's axis in the plane $\psi = 0$ at $x = -14$. The nozzle shape is the same as before, (68) with $r_m = 2\sqrt{2}$. In this and in the following nonaxisymmetric examples, we use the two terms $\Phi_0$ and $\Phi_1$ in the Fourier expansion (12) of the surface pipe potential, and the sphere's potential (10) is truncated at $n = m = 5$. We show

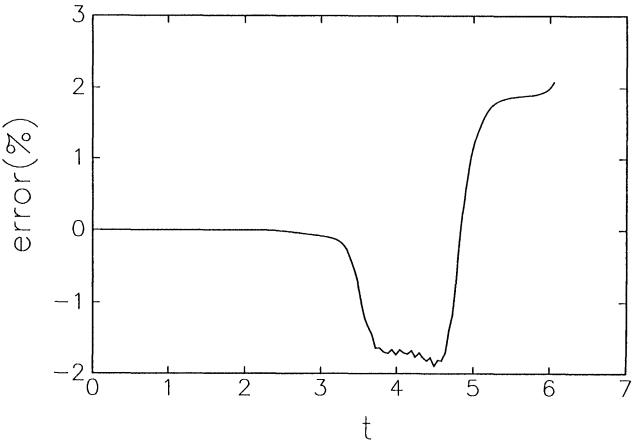


FIG. 7. *Energy error* (73) *versus time for the buoyant sphere in a nozzle of the previous figure.*

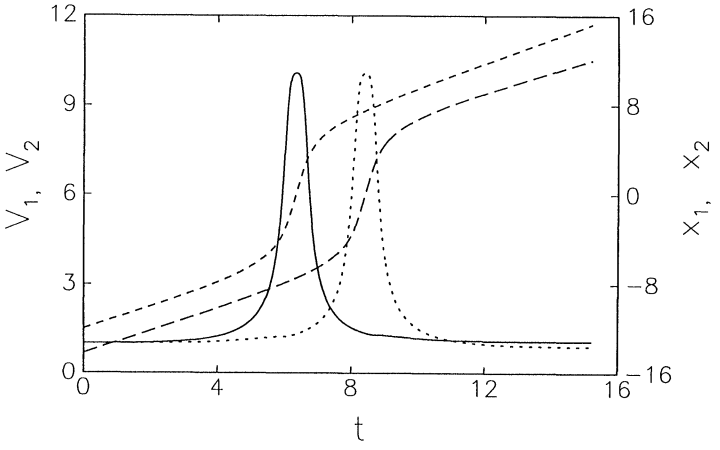


FIG. 8. *Velocities* (*solid and dotted lines, left vertical scale*) *and positions* (*broken lines, right vertical scale*) *of two spheres convected along the axis of the nozzle* (68) *with a minimum radius* $r_m = 2\sqrt{2}$ *sphere radii. The initial separation between the centers is* 2.2 *radii.*

in Fig. 10(a) the $x$- and $y$-components of the velocity of the sphere as a function of time, and in Fig. 10(b) the sphere's trajectory in the $(x, y)$ plane. In the latter figure, the dots on the line are placed at integral values of the dimensionless time starting with $t = 0$. The calculation has been terminated when the sphere reached the downstream boundary of the computational domain $x_d = 14$. It is seen that, after going through the nozzle's throat, the sphere retains a small negative velocity in the direction transverse to the axis so that it eventually hits the pipe's surface. In this case, it was also possible to test with what accuracy the Fourier coefficient of the expansion of the potential on the pipe's wall vanishes at the point $x_d$ (cf. comments in §3.3). We show in Fig. 11 a graph of $\Phi_1(x_d)$ as a function of time as calculated from (38). The value is very small initially and tends to increase somewhat as the sphere advances toward the point $x_d$, as expected. However, the maximum remains of the order of $10^{-3}$, much smaller than the magnitude of $\Phi_0(x_d)$, which is of the order of $10^2$. This case lends itself to another test. Since the pipe we consider is axisymmetric,

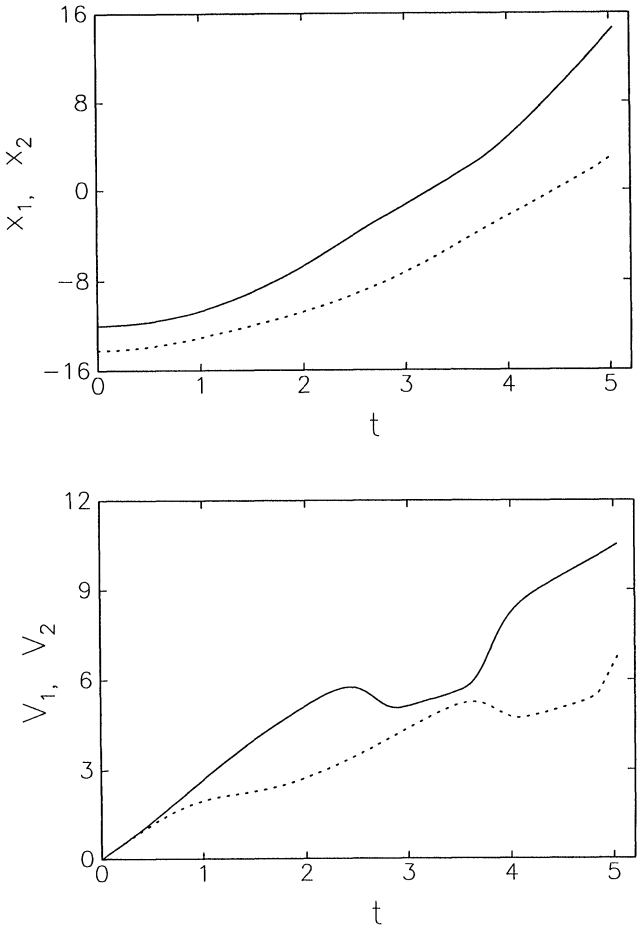


FIG. 9. *Positions* (a) *and velocities* (b) *of two buoyant spheres rising along the axis of the nozzle* (68) *with* $r_m = 1.5$ *sphere radii. The initial separation between the centers is* 2.2 *radii.*

the motion of the sphere must be the same if the initial condition is rotated by any angle around the axis. To check this property, we have run the same case, but this time initially placing the sphere on the plane $\psi = \pi$. The position at the end of the simulation time was the same as before within $2.3\times10^{-2}$ percent.

In Fig. 12, the dotted lines show the trajectories of two spheres in the nozzle (68) with $r_u = 6$ and $r_m = 3\sqrt{2}$, which is indicated here by the solid lines. Initially, the spheres are placed on a line perpendicular to the axis at three units on either side of it. As a consequence of the flow constriction, they acquire a relative velocity that causes them to collide. The calculation was stopped at that point. The precise symmetry of the figure about the axis gives further confidence in the correctness of the calculation. As before, the dots mark the position at integral values of the dimensionless time.

Finally, we consider the gravity-induced motion of three spheres in an unbounded liquid. The initial geometry is shown in Fig. 13. The spheres' centers are in a plane parallel to the acceleration of gravity, and the initial distance from the center of the central sphere is $d = 4$. Figure 14 shows the trajectories for $\theta_1(0) = 40°, \theta_2(0) = 130°$, while Fig. 15 is for $\theta_1(0) = 70°, \theta_2(0) = 130°$. It, can be seen that, in the first case, spheres 2 and 3 collide, while, in the second case, collision occurs between spheres 1

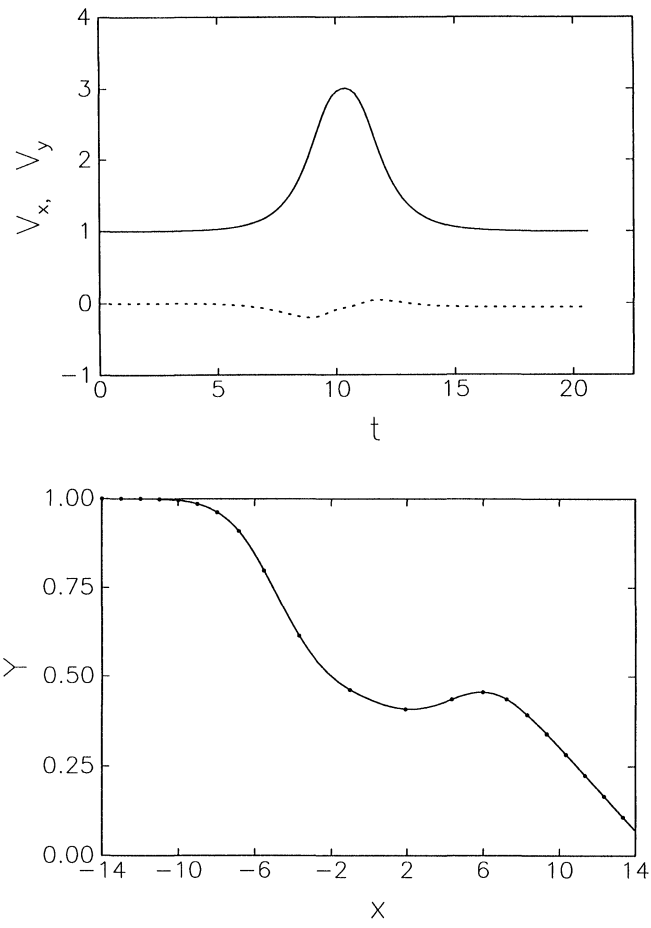


FIG. 10. *Velocity components* (a) *and trajectory* (b) *of a sphere convected through the nozzle* (68) *with* $r_m = 2\sqrt{2}$ *radii. Initially, the sphere is located off axis at* $x = -14, y = 1$. *The dots in* (b) *indicate positions at integral values of the dimensionless time.*

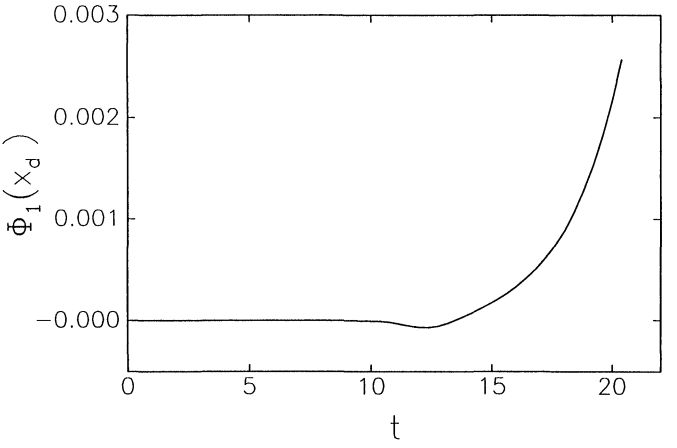


FIG. 11. *Values of the coefficient* $\Phi_1$ *at the downstream section given by* (38) *versus time for the case of the previous figure. The exact value is zero.*

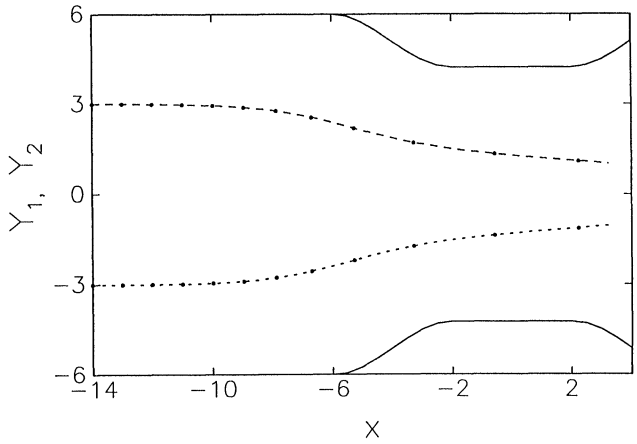


FIG. 12. *Trajectories (broken lines) of two spheres convected through the nozzle* (68) *with* $r_m = 3\sqrt{2}$ *sphere radii (solid lines). Initially, the spheres' centers are on the* $(x, y)$ *plane three units from the axis. The dots indicate positions at integral values of the dimensionless time.*

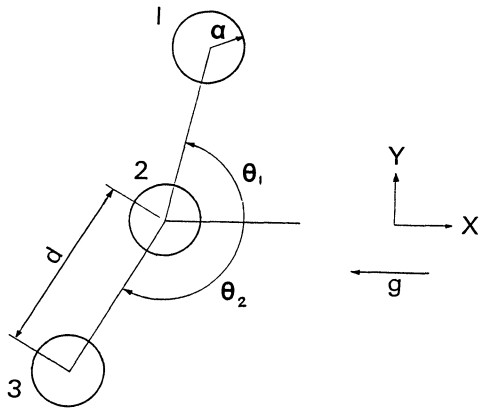


FIG. 13. *The initial configuration of the three-sphere problem studied in Figs.* 14 *and* 15.

and 2. The points indicate positions at integral values of the dimensionless time.

A final comment is in order on the calculation times required for the examples described above. Typically, they were of the orders of several to many hours on a Sun Sparcstation. However, no attempt was made at this stage to optimize the calculation procedure, e.g., by systematically using a variable number of terms in the expansions. It may be expected that an effort in this direction would pay off with a considerable reduction in computation time, as would, of course, recourse to a supercomputer.

**9. Discussion and conclusion.** We have developed a technique to calculate the motions of arbitrarily configured spheres in potential flow through an axisymmetric pipe or in an unbounded liquid. The method can be used to study the inertial coupling among the spheres and ultimately gain insight into the proper formulation of averaged equations. This line of research will be pursued in future publications. In this paper, we have only considered very simple examples for illustration purposes.

In conclusion, we present comments on future work that is needed to improve the mathematical model. In the first place, for application to bubbles, the spheres

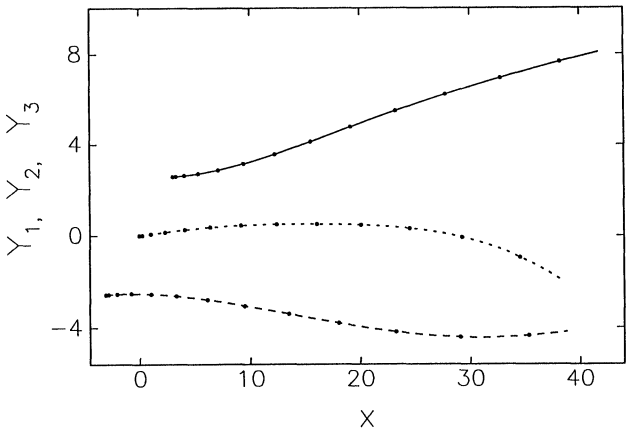


FIG. 14. *Trajectories of the three buoyant spheres shown in Fig.* 13 *for the case where* $\theta_1(0) = 40°, \theta_2(0) = 130°$. *Initially, the two outer spheres are at* 4 *radii from the central one. The dots indicate positions at integral values of the dimensionless time. Note that spheres* 2 *and* 3 *are predicted to collide.*

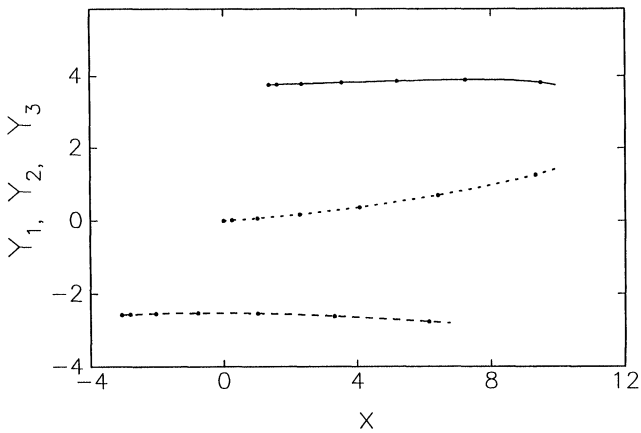


FIG. 15. *Trajectories of the three buoyant spheres shown in Fig.* 13 *for the case where* $\theta_1(0) = 70°, \theta_2(0) = 130°$. *Initially, the two outer spheres are at* 4 *units from the central one. The dots indicate positions at integral values of the dimensionless time. Note that spheres* 1 *and* 2 *are predicted to collide.*

should be allowed to change their volume and to deform. The first objective can be obtained relatively easily by adding one degree of freedom per sphere, while the second objective requires a considerable increase in the number of degrees of freedom per particle and may not be worth pursuing until further progress on the spherical case has been made.

Second, a method must be found to handle collisions between spheres or with the pipe's wall. These events happen necessarily in the present model due to the basic Bernoulli effect of pressure decreases associated to velocity increases. The velocity on the side of a sphere close to another sphere or the tube's wall is higher than on the other side, so that an attractive force develops. The presence of this attractive

force for the case of two spheres moving perpendicularly to their line of centers is well known (see, e.g., Milne-Thomson [25]). In this work, we have encountered several such occurrences, and we had to stop the calculation just before the collision took place. We plan to implement the method recently developed by Sangani and Yao [33] to solve this problem.

Third, it would be desirable to model the drag forces acting on the spheres. We can do this in an approximate way for slip-free spheres at large Reynolds numbers on the basis of work of Kang and Leal [22] and Sangani, Zhang, and Prosperetti [34]. The basic idea is to exploit the relative weakness of the viscous boundary layer that develops around the spheres in these conditions and to calculate the viscous correction to the flow ignoring the interaction among neighboring spheres.

Clearly, the model we have described is a far cry from anything that could be called "realistic." However, computers are expected to become increasingly more powerful, and it is important to start developing now tools to point the way for more physical simulations when they will become feasible.

**Appendix.** We now provide analytical details on some of the results quoted in the text.

*Functions $\Psi_l$ and $\tilde{\Psi}_l$.* The functions $\Psi_l$ and $\tilde{\Psi}_l$ are defined in (17) and (18). To calculate the integral (17), we begin by noting that, referring the points $\mathbf{x}$ and $\mathbf{x}'$ to the cylindrical coordinate system defined after (7), we have

$$\mathbf{x} = (x, r, \psi), \qquad \mathbf{x}' = (x', r', \psi').$$

The distance between $\mathbf{x}$ and $\mathbf{x}'$ is given by

$$|\mathbf{x} - \mathbf{x}'| = R = \left[(x' - x)^2 + r'^2 + r^2 - 2rr' \cos(\psi - \psi')\right]^{1/2}. \tag{A.1}$$

The normal derivative appearing in the integrand of (17) is then

$$\frac{\partial}{\partial n'} \frac{1}{|\mathbf{x} - \mathbf{x}'|} = \frac{1}{R^3} \left\{(x' - x) \sin \eta - [r' - r\cos(\psi' - \psi)] \cos \eta\right\}, \tag{A.2}$$

with $\eta$ as defined in Fig. 2. With the change of variable $\psi' - \psi = 2u$, the integration over $\psi$ yields

$$\Psi_l = -\frac{2\pi\Phi_l\epsilon_l}{A^{3/2}} \int_0^\pi \frac{\cos 2lu(-\sin\eta(x' - x) + \cos\eta(r' - r\cos 2u))}{(1 - m\cos^2 u)^{3/2}}\, du, \tag{A.3}$$

while the other term multiplied by $\tilde{\Phi}_l$ vanishes. With the definitions,

$$A = (x' - x)^2 + (r' + r)^2, \qquad m = 4r'r/A.$$

Equation (A.3) can be rewritten as

$$\Psi_l = -2\pi\epsilon_l \frac{1 - \cos l\pi}{A^{3/2}} B^l(x, x', r, r')\ \Phi_l(x'), \tag{A.4}$$

where

$$B^l(x, x', r, r') = [-(x' - x) \sin \eta + (r' + r) \cos \eta] I_l(m), \tag{A.5}$$

$$- 2r\ J_l(m) \cos \eta, \tag{A.6}$$

with

$$I_l(m) = \int_0^{\pi/2} \frac{\cos 2lu\, du}{(1 - m\sin^2 u)^{3/2}}, \tag{A.7}$$

$$J_l(m) = \int_0^{\pi/2} \frac{\cos^2 u \cos 2lu\, du}{(1 - m\sin^2 u)^{3/2}}. \tag{A.8}$$

These integrations can be carried out in closed form and the results expressed in terms of the complete elliptic integrals of the first and second kind, $K(m)$ and $E(m)$. To this end, we define

$$Q_n = \int_0^{\pi/2} \frac{\cos^{2n} u\, du}{(1 - m\,\sin^2 u)^{3/2}} \tag{A.9}$$

and note the recurrence relation, valid for $n \geq 2$,

$$\begin{aligned} Q_{n+1} = &\left[\frac{2(n-1)}{2n-1}\left(2 - \frac{3}{m}\right) - 1\right] Q_n \\ &+ \frac{1}{2n-1}\left[(2n-3)\left(\frac{3}{m} - 2\right) - 2(n-1)\left(2 - \frac{3}{m} + \frac{2}{m^2}\right)\right] Q_{n-1} \\ &+ \frac{2n-3}{2n-1}\left(1 - \frac{3}{m} + \frac{2}{m^2}\right) Q_{n-2}. \end{aligned} \tag{A.10}$$

This relation is obtained by differentiation from the known recurrence

$$M_n = 2\frac{n-1}{2n-1}\frac{2m-1}{m} M_{n-1} + \frac{2n-3}{2n-1}\frac{1-m}{m} M_{n-2}, \tag{A.11}$$

where

$$M_n = \int_0^{\pi/2} \frac{\cos^{2n} u\, du}{(1 - m\,\sin^2 u)^{1/2}}. \tag{A.12}$$

Together with the explicit values

$$Q_0 = \frac{E(m)}{1-m}, \qquad Q_1 = \frac{K(m) - E(m)}{m}, \tag{A.13}$$

$$Q_2 = \frac{1}{m^2}\left[(2-m)\,E(m) - 2(1-m)\,K(m)\right], \tag{A.14}$$

which readily follow from

$$M_0 = K(m), \qquad M_1 = \frac{1}{m}\left[E(m) - (1-m)\,K(m)\right], \tag{A.15}$$

(A.10) enables us to calculate $Q_n$ for any $n$. With this result and by use of the expansion

$$\cos 2lu = \sum_{n=0}^{l} a_n \cos^{2n} u, \tag{A.16}$$

where the $a_n$'s are the coefficients of the Chebyshev polynomial of degree $2l$ and are given by

$$a_l = 2^{2l-1}, \quad a_n = (-1)^{l-n}\frac{2l}{l-n}\frac{2^{n-1}}{(2n)!}\frac{(l+n-1)!}{(l-n-1)!}, \quad 0 \le n \le l-1, \tag{A.17}$$

we readily obtain the following expression for $I_l(m)$:

$$I_l(m) = \sum_{n=0}^{l} a_n Q_n(m). \tag{A.18}$$

With the above results, it is also obvious that

$$J_l(m) = \sum_{n=0}^{l} a_n Q_{n+1}. \tag{A.19}$$

In particular, the values corresponding to $l = 0$ and $l = 1$ are

$$\begin{aligned} I_0(m) &= \frac{E}{m_1}, \\ I_1(m) &= \frac{2}{m}(K-E) - \frac{E}{m_1}, \\ J_0(m) &= \frac{K-E}{m}, \\ J_1(m) &= \frac{1}{m^2}\left[(3+m_1)E - (1+3m_1)K\right], \end{aligned} \tag{A.20}$$

where $m_1 = 1 - m$.

Note that, when $|\mathbf{x}' - \mathbf{x}| = O(\epsilon)$, $I_l$ and $J_l$ become singular as

$$I_l = O\left(\frac{1}{\epsilon^2}\right), \qquad J_l = O(\log \epsilon).$$

However, the coefficient of $I_l$ in (A.5) becomes $O(\epsilon^2)$, so that product of $I_l$ and its coefficient becomes $O(1)$. Therefore, when $|\mathbf{x}' - \mathbf{x}| = O(\epsilon)$, $B^l(x, x', r')$ behaves asymptotically as $O(\log \epsilon)$, which is integrable.

On the downstream section $S_d$, the function $B^l(x, x', r, r')$ simplifies to

$$B^l(x, x') = (x_d - x) I_l. \tag{A.21}$$

A calculation similar to the preceding one shows that

$$\tilde{\Psi}_l = -4\pi \frac{\cos l\pi}{A^{3/2}} B^l(x, x', r, r') \tilde{\Phi}_l(x'). \tag{A.22}$$

*Translation of the spherical harmonics.* Consider the three points $O, P$, and $Q$, two polar coordinate systems centered at $O$ and $Q$, and let

$$P - Q = (r', \theta', \psi'), \quad P - O = (r, \theta, \psi), \quad Q - O = (\rho, \alpha, \beta). \tag{A.23}$$

When $r > \rho$, the spherical harmonics referred to the origin $Q$ can be expressed in terms of the spherical harmonics referred to the origin $O$ as follows:

$$\frac{P_N^M(\cos\theta')\cos M\psi'}{r'^{N+1}} = \sum_{n=0}^{\infty} \frac{\rho^n}{r^{N+n+1}}$$

$$\cdot\left\{\sum_{m=0}^{n} A_{nm}^{NM}\, P_n^m(\cos\alpha)\, P_{n+N}^{m+M}(\cos\theta)\, \cos[(M+m)\psi - m\beta]\right.$$

$$\left. + \sum_{m=1}^{n} B_{nm}^{NM}\, P_n^m(\cos\alpha)\, P_{n+N}^{|M-m|}(\cos\theta)\, \cos[(M-m)\psi + m\beta]\right\}, \tag{A.24}$$

while, when $r < \rho$,

$$\frac{P_N^M(\cos\theta')\cos M\psi'}{r'^{N+1}} = (-1)^N \sum_{n=0}^{\infty} \frac{r^n}{\rho^{N+n+1}}$$

$$\cdot\left\{\sum_{m=0}^{n} A_{nm}^{NM}\, P_n^m(\cos\theta)\, P_{n+N}^{m+M}(\cos\alpha)\, \cos[(M+m)\beta - m\psi]\right.$$

$$\left. + \sum_{m=1}^{n} B_{nm}^{NM}\, P_n^m(\cos\theta)\, P_{n+N}^{|M-m|}(\cos\alpha)\, \cos[(M-m)\beta + m\psi]\right\}, \tag{A.25}$$

where the constants are given by

$$A_{nm}^{NM} = \frac{(n+N-m-M)!}{(n+m)!(N-M)!}, \tag{A.26}$$

$$B_{nm}^{NM} = (-1)^{\min(M,m)} \frac{(n+N-|M-m|)!}{(n+m)!(N-M)!}. \tag{A.27}$$

Similar expressions hold for the expansion of $P_N^M(\cos\theta')\sin M\psi'/r'^{N+1}$, except that the cosine functions of $\psi$ and $\beta$ in the right-hand sides of (A.24) and (A.25) must be replaced by sine functions.

**Acknowledgments.** The authors are grateful to Prof. A. S. Sangani for several useful discussions and to Dr. Oğuz for helping with the formulation and for providing his numerical results on the surface potential in the pipe.

## REFERENCES

[1] F.F. Abraham, *Computational statistical mechanics. Methodology, applications, and supercomputing*, Adv. Phys., 35 (1986), pp. 1–111.

[2] S. Banerjee, *Separated flow models—II. Higher-order dispersion effects in the averaged formulation*, Internat. J. Multiphase Flow, 6 (1980), pp. 241–248.

[3] A. B. Bassett, *A Treatise on Hydrodynamics*, Vol. I, Leighton, Bell and Co., London, 1888, p. 248; reprinted by Dover, New York, 1961.

[4] G. K. Batchelor and J. T. Green, *The determination of the bulk stress in a suspension of spherical particles to order $c^2$*, J. Fluid Mech., 56 (1972), pp. 401–427.

[5] A. Biesheuvel and S. Spoelstra, *The added mass coefficient of a dispersion of spherical gas bubbles in liquid*, Internat. J. Multiphase Flow, 15 (1989), pp. 911–924.

[6] A. Biesheuvel and L. van Wijngaarden, *The motion of pairs of gas bubbles in a perfect liquid*, J. Engrg. Math., 4 (1982), pp. 349–365.

[7] ———, *Two-phase flow equations for a dilute dispersion of gas bubbles in liquid*, J. Fluid Mech., 148 (1984), pp. 301–338.

[8] J. A. Bouré, *Two-Phase Flow Models: The Closure Issue*, Multiphase Science and Technology, Vol. 3, Hemisphere, Washington, DC, 1987, pp. 3–25.

[9] J. F. BRADY AND G. BOSSIS, *Stokesian dynamics*, Ann. Rev. Fluid Mech., 20 (1988), pp. 111–157.
[10] R. CAFLISCH, M. J. MIKSIS, G. PAPANICOLAOU, AND L. TING, *Effective equations for wave propagation in bubbly liquids*, J. Fluid Mech., 153 (1985), pp. 259–273.
[11] ———, *Wave propagation in bubbly liquids at finite volume fraction*, J. Fluid Mech., 160 (1985), pp. 1–14.
[12] C. S. CAMPBELL, *The stress tensor for simple shear flows of a granular material*, J. Fluid Mech., 203 (1989), pp. 449–473.
[13] D. A. DREW, *Mathematical modeling of two-phase flow*, Ann. Rev. Fluid Mech., 15 (1983), pp. 261–291.
[14] D. A. DREW AND R. T. WOOD, *Overview and taxonomy of models and methods*, in Proc. First Internat. Workshop Two-Phase Flow Fundamentals, Gaithersburg, MD, 1985.
[15] L. DURLOFSKY, J.F. BRADY, AND G. BOSSIS, *Dynamic simulation of hydrodynamically interacting particles*, J. Fluid Mech., 180 (1987), pp. 21–49.
[16] L. GREENGARD AND V. ROKHLIN, *Rapid Evaluation of Potential Fields in Three Dimensions*, Tech. Report 515, Yale Computer Science Dept., Yale University, New Haven, CT, 1987.
[17] E. J. HINCH, *An averaged-equation approach to particle interactions in a fluid suspension*, J. Fluid Mech., 83 (1977), pp. 695–720.
[18] R. W. HOCKNEY AND J. W. EASTWOOD, *Computer Simulation Using Particles*, Hilger, Bristol, UK, 1988.
[19] W. G. HOOVER, *Molecular Dynamics*, Lecture Notes in Physics, Vol. 258, Springer-Verlag, Berlin, 1986.
[20] M. ISHII, *Thermo-Fluid Dynamic Theory of Two-Phase Flow*, Eyrolles, Paris, 1975.
[21] A. V. JONES AND A. PROSPERETTI, *On the suitability of first-order differential models for two-phase flow prediction*, Internat. J. Multiphase Flow, 11 (1985), pp. 133–148.
[22] I. S. KANG AND L. G. LEAL, *The drag coefficient for a spherical bubble in a uniform streaming flow*, Phys. Fluids, 31 (1988), pp. 233–237.
[23] S. KARRILA AND S. KIM, *Foundations of Parallel Computational Microhydrodynamics: The Completed Double Layer Boundary Integral Equation Method*, Rheology Research Center, University of Wisconsin–Madison, Report No. 123, February 1990.
[24] J. B. W. KOK, *Dynamics of Gas Bubbles Moving Through Liquid*, Ph.D. thesis, Twente University, the Netherlands, 1990.
[25] L. M. MILNE-THOMSON, *Theoretical Hydrodynamics*, 4th ed., Macmillan, New York, 1960, pp. 501–506.
[26] R. I. NIGMATULIN, *Spatial Averaging in the Mechanics of Heterogeneous and Disperse Systems*, Internat. J. Multiphase Flow, 5 (1979), pp. 353–385.
[27] A. PROSPERETTI AND A. V. JONES, *The linear stability of general two-phase flow models*, Internat. J. Multiphase Flow, 13 (1987), pp. 161–171.
[28] J. RUBINSTEIN, *Effective equations for flow in random porous media with a large number of scales*, J. Fluid Mech., 170 (1986), pp. 379–383.
[29] A. S. SANGANI, *A pairwise interaction theory for determining the linear acoustic properties of dilute bubbly liquids*, J. Fluid Mech., 232 (1991), pp. 221–284.
[30] ———, *Sedimentation in ordered emulsions of drops at low Reynolds numbers*, Z. Agnew. Math. Phys., 38 (1987), pp. 542–556.
[31] A. S. SANGANI AND A. ACRIVOS, *Slow flow through a periodic array of spheres*, Internat. J. Multiphase Flow, 8 (1982), pp. 343–360.
[32] A. S. SANGANI AND A. K. DIDWANIA, *Dynamic simulations of flows of bubbly liquids at large Reynolds numbers*, J. Fluid Mech., 1992, to appear.
[33] A. S. SANGANI AND C. YAO, *Bulk thermal conductivity of composites with spherical inclusions*, J. Appl. Phys., 63 (1988), pp. 1334–1341.
[34] A. S. SANGANI, D. Z. ZHANG, AND A. PROSPERETTI, *The added mass, Bassett, and viscous drag coefficients in non-dilute bubbly liquids undergoing small-amplitude oscillatory motion*, Phys. Fluids, A3 (1991), pp. 2955–2970.
[35] O. R. WALTON AND R. L. BRAUN, *Stress calculations for assemblies of inelastic spheres in uniform shear*, Acta Mech., 63 (1986), pp. 73–86.
[36] L. VAN WIJNGAARDEN, *Hydrodynamic interaction between gas bubbles in liquid*, J. Fluid Mech., 77 (1976), pp. 27–44.